Synoptic-Scale Environments of Predecessor Rain Events Occurring East of the Rocky Mountains in Association with Atlantic Basin Tropical Cyclones*

BENJAMIN J. MOORE

Cooperative Institute for Research in Environmental Sciences, University of Colorado, and NOAA/Earth System Research Laboratory, Boulder, Colorado

LANCE F. BOSART AND DANIEL KEYSER

Department of Atmospheric and Environmental Sciences, University at Albany, State University of New York, Albany, New York

MICHAEL L. JUREWICZ

NOAA/NWS Forecast Office, Binghamton, New York

(Manuscript received 20 June 2012, in final form 23 September 2012)

ABSTRACT

The synoptic-scale environments of predecessor rain events (PREs) occurring to the east of the Rocky Mountains in association with Atlantic basin tropical cyclones (TCs) are examined. PREs that occurred during 1988–2010 are subjectively classified based upon the synoptic-scale upper-level flow configuration within which the PRE develops, with a focus on the following: 1) the position of the jet streak relative to the TC, 2) the position of the jet streak relative to trough and ridge axes, and 3) the positions of trough and ridge axes relative to the PRE and to the TC. Three categories were identified from this classification procedure: ''jet in ridge,'' ''southwesterly jet,'' and ''downstream confluence.'' PRE-relative composite analysis for each category reveals that, consistent with previous studies, PREs typically occur near a low-level baroclinic zone, beneath the equatorward entrance region of an upper-level jet streak, and in the presence of a stream of water vapor from a TC. Despite these common characteristics, key differences exist among the three PRE categories related to the phasing of a TC with the synoptic-scale flow and to the interactions between a TC and its environment. Brief case studies of PREs associated with TC Rita (2005), TC Wilma (2005), and TC Ernesto (2006) are presented as specific examples of the three PRE categories.

1. Introduction

a. Overview and motivation

A predecessor rain event (PRE), originally defined by Cote (2007, hereafter C07), is an organized area of heavy rainfall [rainfall rates $\geq$100 mm (24 h)$^{-1}$] that develops in connection with water vapor originating in the vicinity of a tropical cyclone (TC), but is separated from the TC by a large distance ($\sim$1000 km). The large water vapor content in the environment of PREs [e.g., precipitable water (PW) values of 40–60 mm] contributed by the TC can favor large rainfall accumulations and flooding, a fact highlighted by recent high-impact flood-producing PREs associated with TC Frances (2004; Galarneau et al. 2010, hereafter GBS10), TC Katrina (2005; C07), TC Erin (2007; GBS10; Schumacher et al. 2011; Schumacher and Galarneau 2012), and TCs Ike and Lowell (2008; Bosart et al. 2012; Schumacher and Galarneau 2012). The flooding impacts of a PRE can be exacerbated when it occurs along the eventual track of its parent TC, saturating soils over which the TC rain shield eventually passes (C07). In addition, consecutive PREs occurring over the same general region during a period of several days can produce widespread heavy rainfall and flooding (Bosart et al. 2012).

* Supplemental information related to this paper is available at the Journals Online website: http://dx.doi.org/10.1175/MWR-D-12-00178.s1.

Corresponding author address: Benjamin J. Moore, NOAA/Earth System Research Laboratory, Physical Sciences Division, Mail Code R/PSD2, 325 Broadway, Boulder, CO 80305.
E-mail: benjamin.moore@noaa.gov

DOI: 10.1175/MWR-D-12-00178.1

Because of the high potential for PREs to cause flooding and adverse societal impacts, accurate forecasting of PREs is imperative. However, accurate forecasts of PREs may be hindered by deficiencies of operational numerical models in predicting convection and heavy rainfall in the warm season (e.g., Fritsch and Carbone 2004; Schumacher and Davis 2010) as well as in representing interactions between TCs and the midlatitude flow (e.g., Atallah and Bosart 2003; Jones et al. 2003). Additionally, it is possible for PREs to take operational forecasters by surprise when attention is directed to other adverse impacts of TCs. Given these forecasting challenges, it is critical that forecasters recognize the synoptic-scale environments, and the key features and processes therein, that are conducive to the development of PREs. In this paper, the synoptic-scale environments of PREs occurring east of the Rocky Mountains are investigated through composite analysis and illustrative case studies, with the ultimate objective of providing key tools and guidance for identifying and predicting PREs.

b. Background on PREs

PREs typically occur when moist air is transported poleward from the vicinity of a TC by strong low-level winds [i.e., a low-level jet (LLJ)] and is forced to ascend (e.g., Bosart and Carr 1978; C07; GBS10). GBS10 and Bosart et al. (2012) noted that PREs are often manifested as heavy-rain-producing mesoscale convective systems (MCSs; e.g., Schumacher and Johnson 2005), developing in flow patterns resembling the classic Maddox et al. (1979) "frontal" type flash-flood pattern. As has been documented for frontal-type MCSs (e.g., Augustine and Caracena 1994; Trier and Parsons 1993; Junker et al. 1999; Moore et al. 2003), PREs have been shown to often involve warm advection and frontogenetically forced ascent at the intersection of an LLJ with a quasi-stationary low-level baroclinic zone and beneath the equatorward entrance region of an upper-level jet streak (C07; GBS10; Bosart et al. 2012). In addition, topographically influenced processes, such as orographic lifting, cold-air damming, and coastal frontogenesis, can contribute to PRE development (C07; Srock and Bosart 2009).

PREs differ from "ordinary" heavy rainfall events due to possible dynamical and thermodynamic influences of a TC. These possible influences of a TC on PRE development can be summarized as follows:

- The synoptic-scale flow transports water vapor from the vicinity of the TC into the PRE region (GBS10; Schumacher et al. 2011; Bosart et al. 2012; Schumacher and Galarneau 2012).
- Strong winds in the TC circulation transport water vapor into the PRE region (e.g., Wang et al. 2009).
- The TC circulation impinges upon a midlatitude baroclinic zone, yielding warm advection, frontogenesis, and ascent, as occurs during extratropical transition (ET; e.g., Klein et al. 2000; Harr and Elsberry 2000; Sinclair 2002; Atallah and Bosart 2003; Jones et al. 2003).
- As commonly occurs during ET, the upper-level diabatic outflow of a TC induces ridge amplification and the intensification of a jet streak immediately downstream of the TC, augmenting divergence and ascent in the equatorward jet entrance region (e.g., Bosart and Lackmann 1995; Sinclair 2002; Klein et al. 2002; Atallah and Bosart 2003; Agustí-Panareda et al. 2004; Archambault 2011, 99–116, 137–138, 144–148).

By definition, all PREs involve the first of the four influences listed above; however, the extent to which the latter three influences are involved in PRE development is a function of the proximity of the TC to the PRE region, the spatial extent of the cyclonic circulation and the upper-level outflow of the TC, and the synoptic-scale flow configuration within which the TC is embedded. The two primary objectives of the current study are 1) to elucidate the different interactions between a TC and its environment through which a PRE can develop, and 2) to examine distinct synoptic-scale flow configurations in which these interactions occur.

The remainder of this paper is organized as follows. Section 2 discusses the data and methods. Section 3 presents a brief summary of the characteristics of PREs during 1988–2010. Section 4 examines the distinct synoptic-scale environments of PREs through PRE-relative composite analysis. Section 5 provides three brief PRE case studies. Last, section 6 provides synthesis and conclusions.

2. Data and methods

a. PRE identification

The PRE database of GBS10, which included PREs during 1995–2008, was extended to include all PREs occurring east of the Rocky Mountains in association with Atlantic basin TCs during 1988–2010 (Table 1). PREs were identified by applying the criteria laid out by GBS10, quoted below:

- Radar reflectivity values $\geq$35 dBZ within a coherent area of rainfall persisting for at least 6 h.
- The average rainfall rate must be $\geq$100 mm (24 h)$^{-1}$ over the entire life of the PRE.
- While there is no objective TC–PRE separation distance required, the following two criteria must be met:

TABLE 1. All documented PREs associated with Atlantic basin TCs during 1988–2010. Listed are key details for each PRE: initiation time and date, geographical area, maximum rainfall amount (rounded to the nearest multiple of 5 mm), location relative to the total observed TC track, and synoptic category. The numbers in parentheses in the synoptic category column correspond to the numbers in Fig. 3. PREs associated with the TCs set in bold were used for the composites. In the event that a TC produced multiple PREs, only the initial PRE was used. For the positions relative to the TC track, LOT refers to left of track, ROT refers to right of track, and AT refers to along track. "N/A" in the maximum rainfall amount column signifies that rainfall observations were not available.

TC (Year)	Initiation time (UTC) and date	Geographical area	Max rainfall amount (mm)	Location relative to the total observed TC track	Synoptic category
Chris (1988)	2100 UTC 28 Aug	PA/NY	75	LOT	SJ (1)
Florence (1988)	1200 UTC 7 Sep	FL/GA/SC/NC	75	ROT	DC (1)
Gilbert (1988)	1200 UTC 16 Sep	MS/AL/TN	140	ROT	UC (1)
Marco (1990)	1200 UTC 10 Oct	GA/SC/NC	200	AT	SJ (2)
Andrew (1992)	0600 UTC 26 Aug	IN/IL	50	LOT	SJ (3)
Arlene (1993)	1200 UTC 18 Jun	KS/NE/IA	110	ROT	JR (1)
Beryl (1994)	1200 UTC 15 Aug	GA/SC/NC/VA	100	AT	DC (2)
Dean (1995)	0000 UTC 1 Aug	OK/KS/MO	80	ROT	SJ (4)
Erin (1995)	0600 UTC 4 Aug	MO/IL	75	LOT	JR (2)
	1500 UTC 4 Aug	OH/PA/NY	60	LOT	JR
Opal (1995)	0000 UTC 3 Oct	TX/LA/AL/GA/NC/VA	200	AT	SJ (5)
Fran (1996)	0500 UTC 4 Sep	NC	100	AT	UC (2)
Danny (1997)	0000 UTC 23 Jul	NC	150	AT	DC (3)
	0500 UTC 24 Jul	NJ/PA	75	LOT	DC
Bonnie (1998)	0400 UTC 26 Aug	PA/NY/NJ/CT	50	LOT	SJ (6)
	1200 UTC 26 Aug	NY/NJ/CT (off coast)	N/A	LOT	SJ
	0300 UTC 27 Aug	NY/NJ/CT (off coast)	N/A	LOT	SJ
Bret (1999)	2000 UTC 23 Aug	NM/TX	40	ROT	UC (3)
Floyd (1999)	1800 UTC 14 Sep	NC/SC	125	LOT	SJ (7)
Harvey (1999)	1600 UTC 20 Sep	GA/SC/NC	70	LOT	SJ (8)
Helene (2000)	1700 UTC 20 Sep	GA/SC	50	AT	SJ (9)
	0500 UTC 21 Sep	GA/SC	75	LOT	SJ
Lili (2002)	1200 UTC 2 Oct	OK/KS/NE/IA	170	LOT	JR (3)
Grace (2003)	0000 UTC 31 Aug	OK/KS/MO/IL/IN	225	LOT	JR (4)
Isabel (2003)	1600 UTC 14 Sep	NC (off coast)	N/A	AT	UC (4)
	0700 UTC 15 Sep	PA/MD/NJ	100	ROT	UC
Alex (2004)	1900 UTC 1 Aug	VA	110	LOT	DC (4)
	1900 UTC 2 Aug	VA	130	LOT	DC
Bonnie (2004)	0500 UTC 12 Aug	GA/NC/SC	90	LOT	SJ (10)
	1700 UTC 12 Aug	PA/NY	150	LOT	SJ
	0300 UTC 13 Aug	ME	75	LOT	SJ
Charley (2004)	0700 UTC 13 Aug	FL/GA/SC	80	LOT	SJ (11)
	2100 UTC 13 Aug	NC/VA	80	LOT	SJ
Gaston (2004)	1100 UTC 30 Aug	NY	60	LOT	SJ (12)
	2000 UTC 30 Aug	NY/VT/NH/ME	90	LOT	SJ
Frances (2004)	0400 UTC 8 Sep	NY/CT	120	ROT	SJ (13)
Jeanne (2004)	0400 UTC 28 Sep	PA/NY/MA	90	LOT	DC (5)
Matthew (2004)	1900 UTC 7 Oct	AS/MO/LA/TX	225	AT	SJ (14)
Dennis (2005)	1600 UTC 9 Jul	AL/GA/SC	75	AT	DC (6)
Irene (2005)	0000 UTC 15 Aug	NY/CT/RI	100	LOT	SJ (15)
Katrina (2005)	1800 UTC 28 Aug	KY/IN/OH	100	AT	DC (7)
	0700 UTC 29 Aug	KY	200	AT	DC
	0000 UTC 30 Aug	NY/PA	75	ROT	DC
	0000 UTC 30 Aug	ME	150	ROT	DC
	0000 UTC 31 Aug	MA/CT/ME	125	ROT	DC
Ophelia (2005)	0300 UTC 15 Sep	NY/VT/NH	50	LOT	SJ (16)
	1000 UTC 15 Sep	NY/CT/RI/MA	80	LOT	SJ
Rita (2005)	2200 UTC 24 Sep	NE/IA/MN/WI	200	LOT	JR (5)
Wilma (2005)	1800 UTC 23 Oct	GA/SC/NC	125	LOT	SJ (17)
Alberto (2006)	1800 UTC 12 Jun	NC/SC	90	AT	DC (8)
Ernesto (2006)	1800 UTC 30 Aug	NC/VA	110	AT	DC (9)
	1200 UTC 31 Aug	NC/TN/KY/WV	100	LOT	DC
Erin (2007)	2100 UTC 18 Aug	MN/IA/WI	350	LOT	JR (6)
Ike (2008)	0000 UTC 13 Sep	KS/MO/IL/IN	200	LOT	JR (7)
Hermine (2010)	1200 UTC 7 Sep	OK/AR	125	ROT	DC (10)

- There must be a clear separation on the radar imagery between the coherent area of rainfall and the TC rain shield.
- Deep tropical moisture directly associated with the TC must be advected away from the TC into the region of the coherent area of rainfall.

Candidate PREs were manually tracked by inspecting national radar reflectivity imagery. For 1988–94, this manual tracking was conducted using the National Oceanic and Atmospheric Administration (NOAA) National Climatic Data Center (NCDC) hourly U.S. Weather Surveillance Radar-1957 (WSR-57) summary charts archived on 35-mm microfilm at the University at Albany, State University of New York (SUNY), Science Library. For 1995–2010, the manual tracking procedure utilized digital national Weather Surveillance Radar-1988 Doppler (WSR-88D) imagery available online from the National Center for Atmospheric Research (NCAR) case selection archive (http://www.mmm.ucar.edu/imagearchive/) and from NCDC (http://www.ncdc.noaa.gov/oa/radar/radardata.html). The WSR-57 imagery is available at a coarse spatial resolution relative to the WSR-88D imagery, and thus introduced uncertainty regarding the structure, intensity, and motion of some PREs. However, we contend that the WSR-57 imagery adequately captured the characteristics of PREs for the purposes of the current study. The time of PRE initiation was recorded as the time at which radar reflectivity values $\geq$35 dBZ first appeared within the PRE. Each PRE was tracked until it weakened and no longer met the $\geq$35-dBZ radar reflectivity threshold, or until it merged with the main TC rain shield and no longer corresponded to a distinct area of rainfall.

Rainfall amounts for PREs that occurred during 2001–10 were determined using the 4-km quantitative precipitation estimates gridded product from the NOAA/National Weather Service (NWS) National Precipitation Verification Unit (http://origin.hpc.ncep.noaa.gov/npvu/). For cases occurring prior to 2001, the NOAA Climate Prediction Center Daily Unified Precipitation Dataset was used. This dataset is gridded at 0.25° horizontal resolution and is available for download from the NOAA/Earth System Research Laboratory (http://www.esrl.noaa.gov/psd/data/gridded/data.unified.html). These gridded datasets were supplemented with observations from the NWS cooperative high-resolution 24-h rain gauge network and the NCDC hourly precipitation dataset, both archived at NCDC (http://www.ncdc.noaa.gov/oa/climate/climatedata.html).

Following GBS10, water vapor transport from a TC to a PRE was assessed for each prospective case by manually examining maps of PW and the synoptic-scale flow generated from the National Centers for Environmental Prediction (NCEP) Climate Forecast System Reanalysis (CFSR; Saha et al. 2010) dataset, which is available at 0.5° × 0.5° horizontal resolution and 6-h temporal resolution for 1979–2010. Observed upper-air and surface charts archived at the NOAA Storm Prediction Center (http://w1.spc.woc.noaa.gov/obswx/maps/) and atmospheric soundings archived at the University of Wyoming (http://weather.uwyo.edu/upperair/sounding.html) were used to verify the gridded analyses.

Key characteristics of each PRE were recorded, including the separation distance between the PRE and its parent TC at the time of PRE initiation ($T - 0$ h), the maximum PRE rainfall amount, PRE longevity, and the location of the PRE relative to the total observed track of the parent TC. The TC track information was obtained from the National Hurricane Center (NHC) Best Track dataset (http://www.nhc.noaa.gov/pastall.shtml).

b. PRE classification and compositing method

A key factor that distinguishes the predominant flow patterns associated with PREs is the configuration of the upper-level jet stream. This factor was recognized by GBS10, who classified PREs by upper-level jet streak curvature in order to distinguish PREs occurring in association with a large-scale upper-level ridge (''anticyclonically curved'' category) from those occurring in association with a large-scale upper-level trough (''cyclonically curved'' category). This classification method, while useful, does not explicitly account for three interrelated factors that we hypothesize have important dynamical implications for PRE development: 1) the position of the upper-level jet streak relative to the TC, 2) the position of the upper-level jet streak relative to upper-level trough and ridge axes, and 3) the positions of upper-level trough and ridge axes relative to the PRE and to the TC. For example, the synoptic-scale flow configurations associated with anticyclonic jet streak curvature can exhibit large case-to-case variability with regard to these three factors, likely causing key features in the environments of PREs to be obscured in composites. To build off of the work of GBS10, we subjectively classified PREs according to the configuration of the synoptic-scale upper-level flow and the embedded jet streak at the time of PRE initiation, focusing on the three interrelated factors listed above.[1] Three categories of PREs were identified from

[1] Plots of the 200-hPa flow pattern associated with each PRE at the 6-h analysis time closest to the time of PRE initiation are provided in the online supplement.

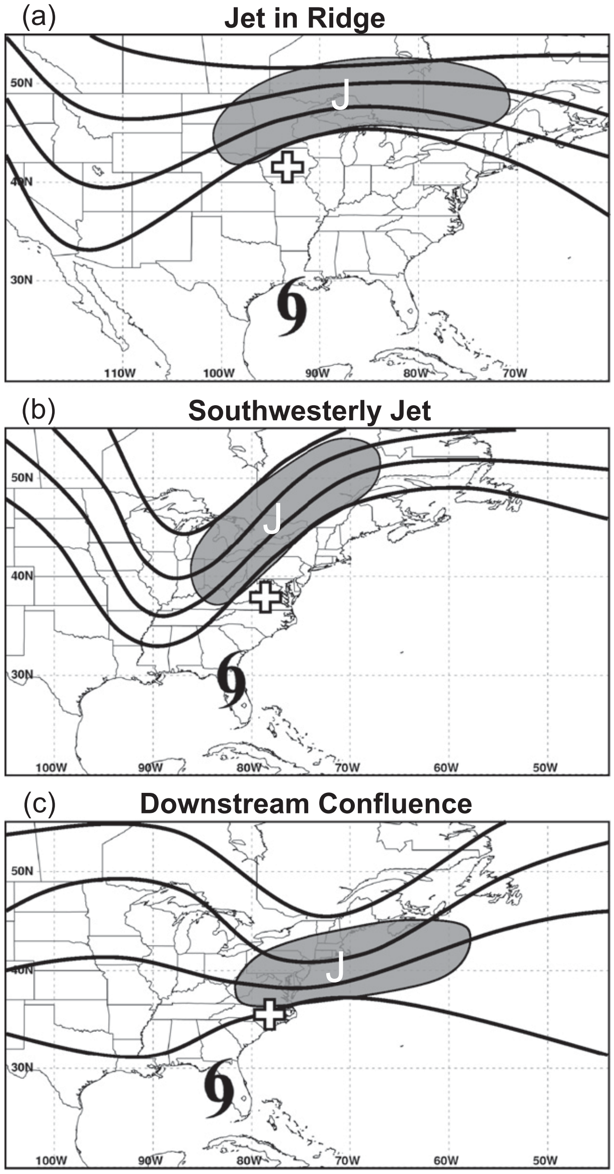

FIG. 1. Schematic illustrations of the characteristic 200-hPa flow configurations for (a) JR, (b) SJ, and (c) DC category PREs. PRE and TC locations are indicated by the "+" symbol and the tropical storm symbol, respectively. The geopotential height contours are shown in black, the jet streak is represented by the gray shaded region, and the location of maximum wind speed is denoted by the "J" symbol.

this classification procedure and are described briefly below.

The first category, jet in ridge (JR; Fig. 1a), features an anticyclonically curved jet streak on the poleward flank of a broad upper-level ridge, beneath which the TC is situated. The second category, southwesterly jet (SJ; Fig. 1b), features a southwesterly jet streak positioned downstream of an upper-level trough that is located immediately upstream and poleward of the TC. For the third category, downstream confluence (DC; Fig. 1c), an upper-level trough is situated downstream and poleward of the TC, and the jet streak is positioned in a region of confluence downstream of the TC. The flow patterns associated with the SJ and DC categories are notably similar to the "northwest" and "northeast" patterns, respectively, identified by Harr et al. (2000) based upon the location of a major upper-level trough relative to TCs undergoing ET (see their Fig. 1). An unclassifiable (UC) category was also included in this classification procedure, consisting of PREs that did not fit into the other three categories. The UC PREs did not appear to develop in connection with an upper-level jet streak and involved mesoscale processes such as orographic lifting or convergence along mesoscale surface boundaries (e.g., coastal fronts, convectively generated outflow boundaries, etc.). For the TCs that produced more than one PRE (Table 1), all of the associated PREs fit into the same category. It is possible for a flow pattern corresponding to one of the three PRE categories to change over time after PRE initiation to resemble another, owing to the movement of the TC and upper-level troughs and ridges. These possible changes are not addressed in the current study as the focus herein is only on the 24-h period centered on the time of PRE initiation.

Synoptic-scale composites were generated for the JR, SJ, and DC categories at 12 h prior to the time of PRE initiation ($T - 12$ h), $T - 0$ h, and 12 h after the time of PRE initiation ($T + 12$ h) using the 6-h NCEP CFSR gridded analyses. The 6-h analysis time closest to the actual $T - 0$ h (Table 1) was used for $T - 0$ h in the compositing. If $T - 0$ h fell exactly halfway between two 6-h analysis times, the later time was used. For the TCs associated with more than one PRE (Table 1), only the initial PRE was used in order to preclude biasing the composites by including multiple PREs associated with same TC. Prior to generating the composites, the grids for each PRE case were shifted such that the PRE centroid at $T - 0$ h (subjectively determined from radar imagery) was collocated with the mean $T - 0$ h PRE centroid location for its respective category. Similar storm-relative compositing methods have proven effective for examining the environments of PREs (GBS10), TCs (Atallah et al. 2007), and MCSs (e.g., Augustine and Caracena 1994; Schumacher and Johnson 2005; Coniglio et al. 2010). Geographic boundaries are shown in the composite maps throughout section 4 for spatial reference and distance scaling purposes only. Because the composites presented in this paper are PRE relative, the apparent geographic placement of key features in the environments of PREs is artificial.

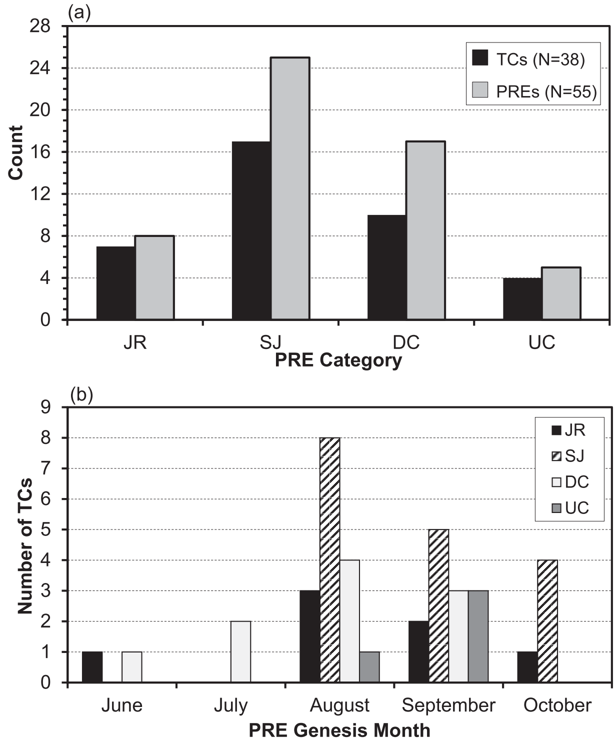

FIG. 2. (a) Distribution of all documented PREs (gray bars) and TCs that produced PREs (black bars) during 1988–2010 binned by category. (b) Monthly absolute frequency distribution of TCs that produced PREs during 1988–2010 binned by the PRE genesis month and separated by category. The bars are shaded according to the legend.

3. Characteristics of PREs during 1988–2010

a. Overview

A total of 55 PREs occurring during 1988–2010 were identified in the United States east of the Rocky Mountains in association with 38 Atlantic basin TCs. The JR category consisted of 7 TCs and 8 PREs, the SJ category consisted of 17 TCs and 25 PREs, the DC category consisted of 10 TCs and 17 PREs, and the UC category consisted of 4 TCs and 5 PREs (Fig. 2a). As these numbers indicate, in contrast to GBS10, who documented only one PRE per TC, we identified a number of TCs that were associated with more than one PRE (Table 1).

PREs occurred preferentially in August and September, and August was the peak month for PREs in the JR, SJ, and DC categories (Fig. 2b). The SJ category PREs tended to occur in the later part of the season, with no PREs occurring prior to August, whereas DC category PREs tended to occur in the earlier part of the season, with 7 of 10 TCs producing PREs in June, July, and August (Fig. 2b). The JR category, containing only seven TCs, appeared to be evenly distributed throughout the season (Fig. 2b).

b. Geographic distribution and TC tracks

The locations of the initial PRE for each TC and the associated TC track are shown in Fig. 3. The dates and TC names associated with the numbered PRE–TC pairs in Fig. 3 can be found in Table 1. For the JR category (Fig. 3a), PREs developed exclusively in the Midwest. The TCs associated with the JR category generally tracked northwestward across the Gulf of Mexico and made landfall along the Gulf of Mexico coast, subsequently recurving over the south-central United States (Fig. 3a). PREs in the SJ category tended to develop in the eastern United States (Figs. 3b,c), with the exception of four PREs (numbers 3, 4, 5, and 14) that developed in the central United States. The TCs associated with the SJ category made landfall along the Gulf of Mexico coast or along the eastern U.S. coast and generally exhibited well-defined recurvature. The DC category PREs developed in the south-central United States and along the eastern U.S. coast, with a cluster of five PREs (numbers 2, 3, 4, 8, 9) developing across the Carolinas and Virginia to the east of the Appalachian Mountains (Fig. 3d). Similar to the TCs associated with the SJ category, TCs associated with the DC category generally made landfall along the Gulf of Mexico coast or along the eastern U.S. coast. Two of the UC PREs (numbers 2 and 4) developed along the eastern U.S. coast in association with TCs making landfall along the southeastern U.S. coast, while the remaining two (numbers 1 and 3) developed over Alabama and northwestern Texas, respectively, in association with TCs that made landfall along the western Gulf of Mexico coast (Fig. 3e).

c. Key properties

Box-and-whisker plots of the separation distance between the PRE and parent TC at $T - 0$ h, maximum PRE rainfall, and PRE longevity are shown in Fig. 4 for the JR, SJ, and DC categories and for all PRE categories (including the UC category) combined. Only the initial PRE associated with each TC was used in tabulating the statistics in Fig. 4. The median separation distance for all PREs was 970 km, with maximum and minimum values of 2160 km (JR category) and 480 km (DC category), respectively (Fig. 4a). The JR PREs generally had the largest separation distances, with a median value of 1120 km compared with 970 and 840 km for the SJ and DC categories, respectively (Fig. 4a). The differences in the separation distance distributions among the three categories are not statistically significant according to a two-sided Student's t test (e.g., see section 5.2.1 in Wilks 2006).

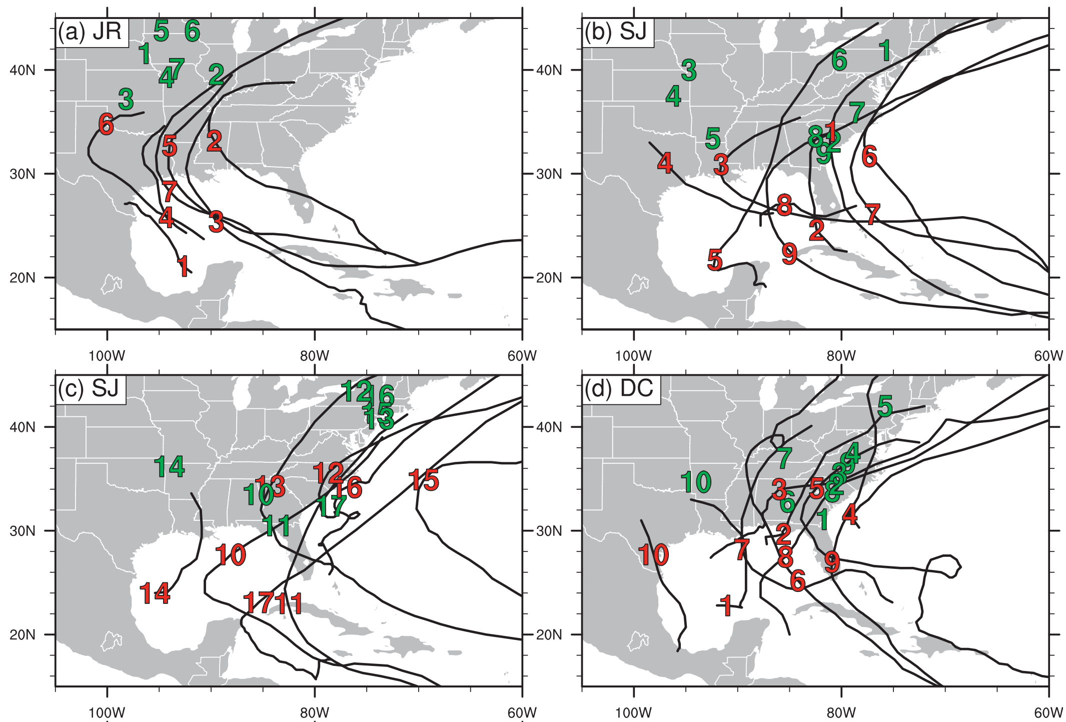

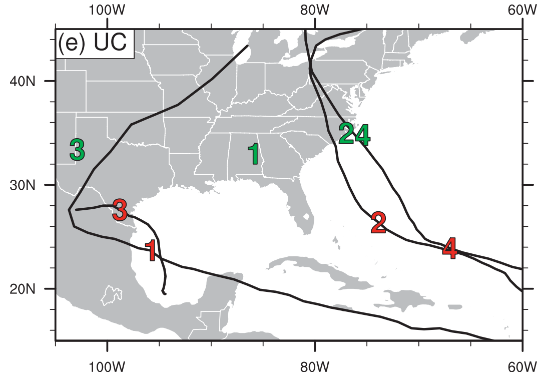

FIG. 3. Plots of TC tracks (black lines) for (a) JR, (b) SJ, (c) SJ, (d) DC, and (e) UC category PREs from the National Hurricane Center Best Track dataset. PRE initiation locations are marked by the green numbers, and the TC locations at the time of PRE initiation are marked by the red numbers. For those TCs that produced multiple PREs, PRE and TC locations are marked only for the initial PRE. The number corresponding to each PRE–TC pair can be found in the synoptic category column of Table 1. Because of the large number of TCs/PREs for the SJ category, two SJ panels are shown for clarity.

The maximum rainfall totals produced by PREs (Fig. 4b) ranged from 40 mm (UC category; not shown) to 350 mm (JR category), and the highest rainfall totals were typically produced by JR PREs (median value of 200 mm). The SJ and DC PREs in general produced considerably smaller maximum rainfall totals than JR PREs, with median values for the two categories of 80 and 100 mm, respectively (Fig. 4b). The differences in the maximum rainfall distributions between the JR and SJ categories and between the JR and DC categories are statistically significant at the 95% level according to a two-sided Student's t test. These significant differences in maximum rainfall can be partially explained by the fact that the JR PREs included in these statistics, except for the TC Erin (1995) PRE, were manifested as long-lived MCSs that were quasi-stationary and featured convective cell training, characteristics favoring large rainfall accumulations. This mesoscale organization is exemplified by the JR PREs associated with TC Erin (2007) and TC Ike (2008), studied in detail by GBS10 and Bosart et al. (2012), respectively. The SJ and DC PREs, by contrast, typically lacked the longevity (Fig. 4c) and the mesoscale organization conducive to producing rainfall totals comparable to those of the JR category.

For all PREs, the median longevity was 17 h, with the longest-lived PREs (48 h) occurring in the JR and SJ categories and the shortest-lived PRE (8 h) occurring in the SJ category (Fig. 4c). The JR category had the greatest median longevity (24 h), substantially longer than those of the SJ and the DC categories (16 and 14 h, respectively; Fig. 4c) and consistent with the tendency of JR PREs to produce the largest maximum rainfall totals. The differences in the longevity distributions among the three categories are not statistically significant according to a two-sided Student's t test.

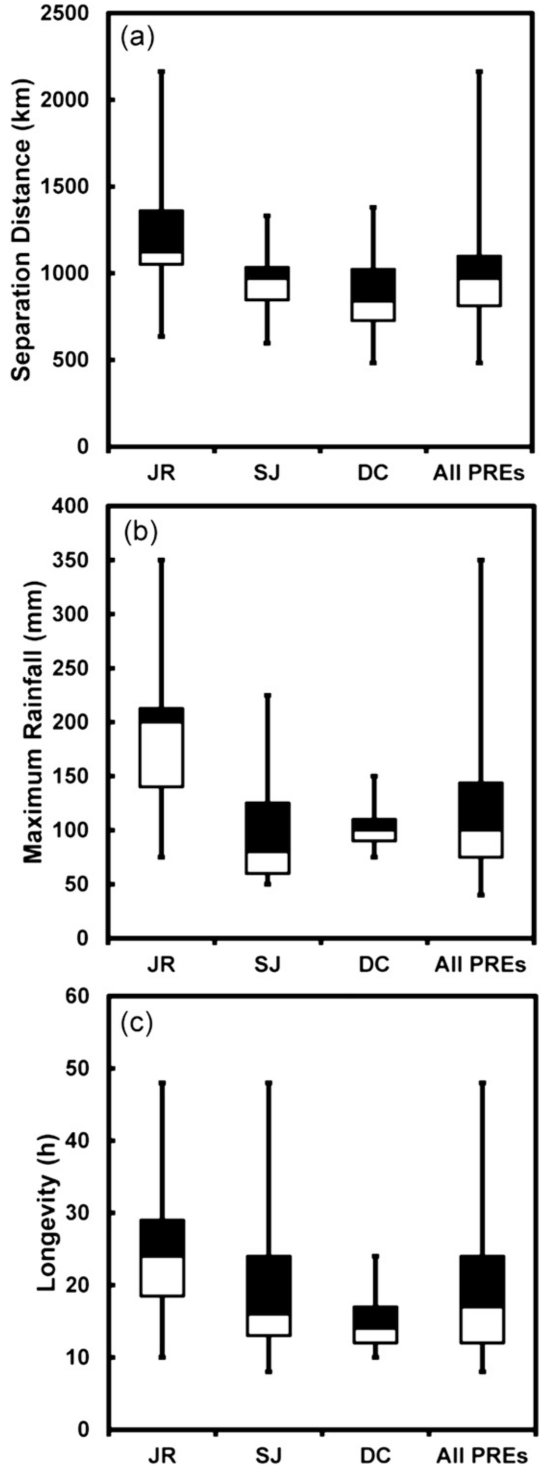

FIG. 4. Box-and-whisker plots for the JR, SJ, and DC category PREs and for all PRE categories combined of (a) separation distance (km) between the TC and PRE at the time of PRE initiation, (b) maximum PRE rainfall (mm), and (c) PRE longevity (h). The whiskers indicate the minimum and maximum values, the bottom (top) of the box marks the first (third) quartile, and the boundary separating the white and black shading denotes the median. Only the initial PRE associated with each TC was included in these statistics.

4. Synoptic-scale environments of PREs

a. JR category

1) SYNOPTIC EVOLUTION

The 200-hPa flow pattern at $T - 12$ h for the JR category features a broad ridge poleward of the composite TC, with an anticyclonically curved 50 m s^{-1} jet streak situated in a region of confluence on the poleward flank of the ridge (Fig. 5a). An inverted sea level pressure (SLP) trough (Figs. 5b) and an associated zonally oriented baroclinic zone are positioned poleward of the TC beneath the equatorward entrance region of the jet streak (Fig. 6a). The baroclinic zone is intersected by 10–12.5 m s^{-1} southerly/southeasterly 925-hPa winds (i.e., an LLJ; Fig. 6a), linked to a corridor of 925-hPa water vapor flux (i.e., the product of the water vapor mixing ratio q_v and the horizontal wind $\mathbf{V}$; Fig. 6b) extending poleward from the TC between the inverted trough and a surface anticyclone to the east (Fig. 5b). Warm advection, frontogenesis, and water vapor flux convergence [evaluated on an isobaric surface as $-\nabla \cdot (q_v\mathbf{V})$] are evident at 925 hPa in the vicinity of a strip of PW values >45 mm at the intersection of the LLJ with the baroclinic zone (Figs. 5b and 6a,b), suggesting that conditions favorable for heavy rainfall already exist at $T - 12$ h. Frontogenesis calculations in the current study were carried out using the Petterssen two-dimensional frontogenesis equation (Petterssen 1936, 1956, 200–202), following the method of Keyser et al. [1988, see their Eqs. (1.1)–(1.4)]. Examination of the composited JR PREs reveals that for each PRE an area of heavy rainfall was present near the PRE region 12–24 h prior to $T - 0$ h, a characteristic that is consistent with the favorability of the environment for heavy rainfall at $T - 12$ h. For instance, as noted by GBS10, the TC Erin (2007) PRE was preceded by a weak MCS, and, as documented by Bosart et al. (2012), the TC Ike (2008) PRE was preceded by a PRE linked to eastern Pacific TC Lowell.

Between $T - 12$ and $T + 12$ h, the 200-hPa jet streak strengthens to 55 m s^{-1} and remains nearly stationary, with the PRE located beneath the equatorward jet entrance region (Figs. 5a,c,e). At $T - 0$ and $T + 12$ h, the PRE is positioned in a region of warm advection and frontogenesis at the intersection of the LLJ and the baroclinic zone (Figs. 6c,e). The frontogenesis occurs in the presence of a pronounced shift in 925-hPa winds from southerly to northeasterly across the baroclinic zone, corresponding to a couplet of warm and cold advection (Figs. 6c,e). Meanwhile, a plume of moist air, featuring PW values >45 mm (Figs. 5d,f) and 925-hPa q_v values >14 g kg^{-1} (Figs. 6d,f), progresses into the PRE region from the eastern flank of the TC, and 925-hPa

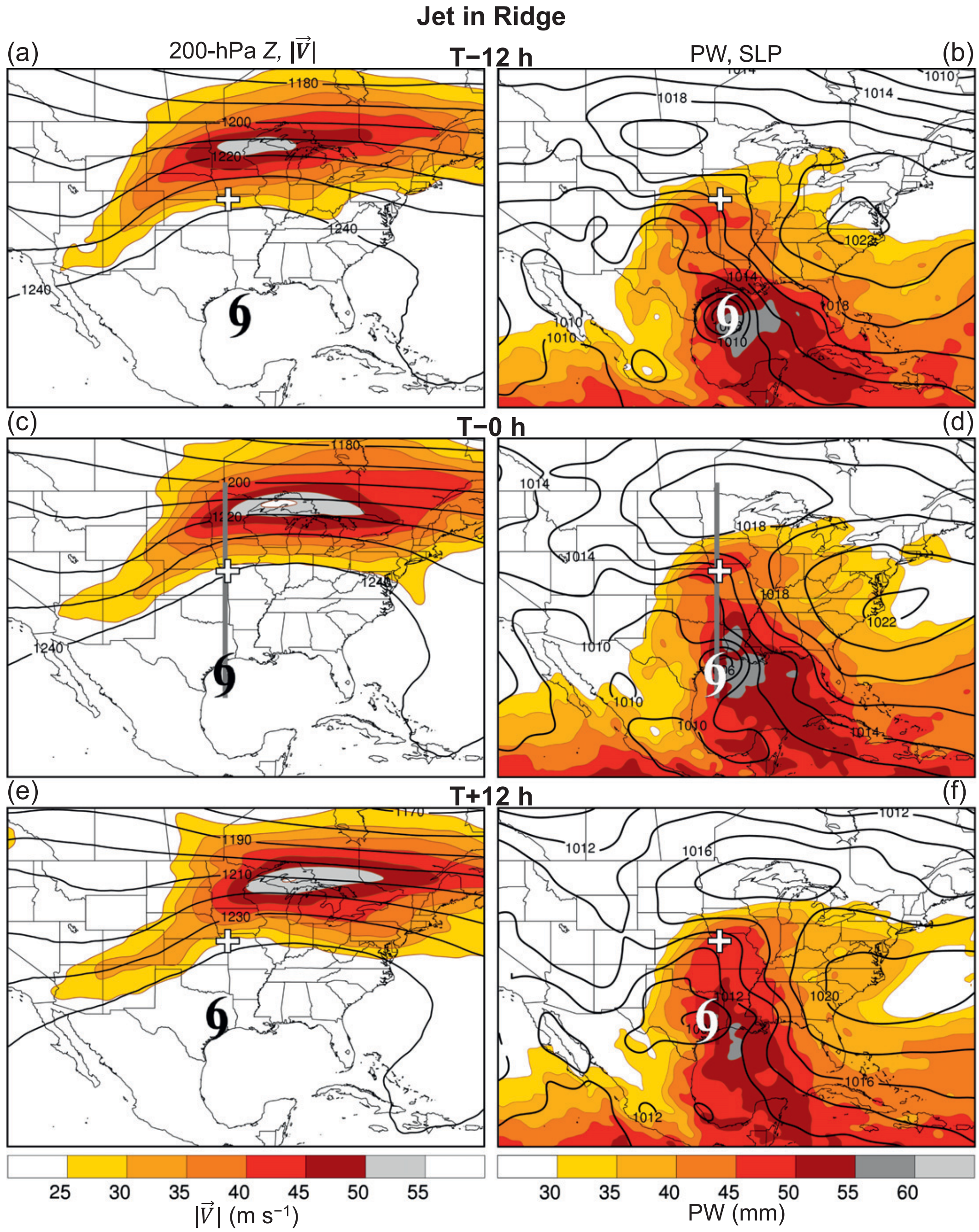

FIG. 5. PRE-relative composites for the seven JR category PREs. (left) 200-hPa geopotential height (contoured in black every 10 dam) and wind speed (shaded in m s^{-1} according to the color bar) for (a) $T - 12$, (c) $T - 0$, and (e) $T + 12$ h. (right) SLP (contoured in black every 2 hPa) and PW (shaded in mm according to the color bar) for (b) $T - 12$, (d) $T - 0$, and (f) $T + 12$ h. The PRE initiation location and the composite TC location are indicated by the "+" symbol and the tropical storm symbol, respectively. The gray lines in (c) and (d) mark the location of the vertical cross section in Fig. 7.

water vapor flux convergence is maintained along the baroclinic zone (Figs. 6d,f).

A north–south composite vertical cross section through the PRE and the TC at $T - 0$ h (Fig. 7) reveals vigorous ascent in the presence of frontogenesis at the terminus of the LLJ and an associated poleward-extending plume of water vapor. Ascent extends up to ~300 hPa along a poleward-sloping region of mid- and upper-level

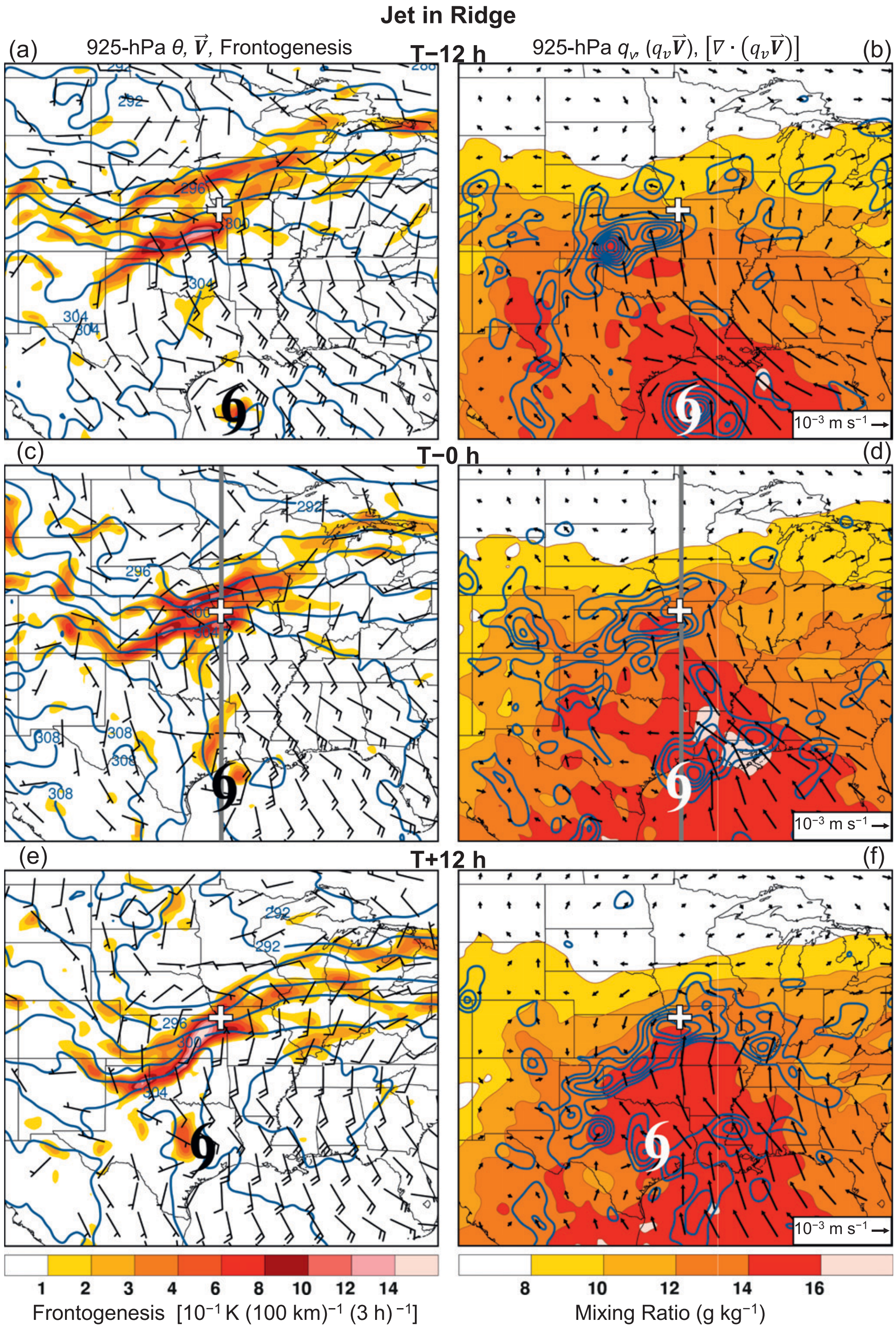

FIG. 6. PRE-relative composites for the seven JR category PREs. (left) 925-hPa potential temperature (contoured in blue every 2 K), wind (plotted for wind speeds ≥2.5 m s^{-1}, half barb: 2.5 m s^{-1}; full barb: 5 m s^{-1}), and Petterssen frontogenesis [shaded in 10^{-1} K (100 km)$^{-1}$ (3 h)$^{-1}$ according to the color bar] for (a) $T - 12$, (c) $T - 0$, and (e) $T + 12$ h. (right) 925-hPa water vapor mixing ratio (shaded in g kg^{-1} according to the color bar), water vapor flux (vectors in 10^{-3} m s^{-1}; vector scale in lower right), and water vapor flux convergence (contoured in blue every 1×10^{-7} s^{-1} starting at 1×10^{-7} s^{-1}) for (b) $T - 12$, (d) $T - 0$, and (f) $T + 12$ h. The PRE initiation location and the composite TC location are indicated as in Fig. 5. The gray lines in (c) and (d) mark the location of the vertical cross section in Fig. 7.

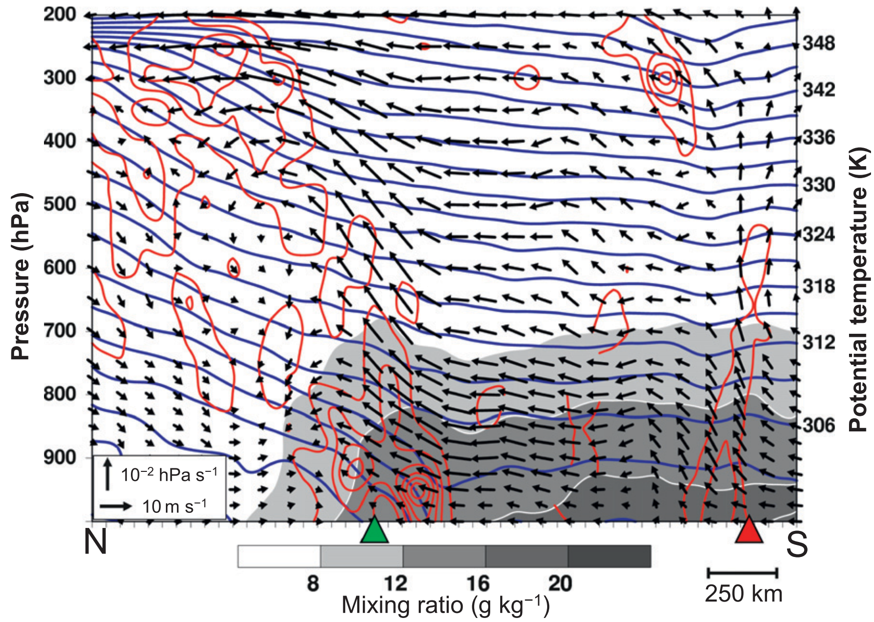

FIG. 7. Composite vertical cross section for the seven JR category PREs at $T - 0$ h along the gray lines in Figs. 5c,d and 6c,d showing potential temperature (contoured in blue every 3 K), Petterssen frontogenesis [contoured in red every 2×10^{-1} K $(100\ \mathrm{km})^{-1}$ $(3\ \mathrm{h})^{-1}$ starting at 1×10^{-1} K $(100\ \mathrm{km})^{-1}$ $(3\ \mathrm{h})^{-1}$], water vapor mixing ratio (shaded in g kg^{-1} according to the gray-scale bar), and flow vectors in the plane of the cross section (horizontal component in m s^{-1} and vertical component in hPa s^{-1}; reference vectors shown in lower left). The latitudinal positions of the PRE and the TC are indicated by the green and red triangles, respectively.

frontogenesis (Fig. 7) beneath the entrance region of the 200-hPa jet streak (Fig. 5c). The configuration depicted at $T - 0$ h in Fig. 7 is similar to that of the ‘‘anticyclonically curved’’ category composite vertical cross section of GBS10 (their Fig. 9).

2) DIABATIC INFLUENCES ON THE UPPER-LEVEL JET

Numerous studies have shown that the upper-level diabatically driven outflow from a heavy precipitation-producing storm system (e.g., extratropical cyclone, TC, MCS, and PRE) can impinge upon a meridional potential vorticity (PV) gradient associated with an upper-level jet streak, inducing upper-level ridge amplification and producing increases in the PV gradient and wind speeds along the jet streak (e.g., Cammas et al. 1994; Riemer et al. 2008; Archambault 2011, 99–116, 137–138, 144–148; Bosart et al. 2012). Following the methods applied by Archambault (2011, p. 137) and Bosart et al. (2012), the interaction between the diabatic outflow associated with the PRE and/or the TC and an upper-level jet is examined with composite maps of PV in the 250–200-hPa layer, 250–200-hPa layer-averaged irrotational wind, negative PV advection by the irrotational wind in the 250–200-hPa layer, and 700–500-hPa layer-averaged ascent (Fig. 8).

At $T - 12$ h, strong ascent is located within a region of low PV (Fig. 8a) and anticyclonic shear in the equatorward entrance region of the 200-hPa jet streak (Fig. 5a), a signature likely related to preexisting areas of heavy rainfall in the composite members. Irrotational winds are directed outward from the region of ascent (a signature of diabatic outflow) across the axis of the jet streak toward larger values of PV, corresponding to negative PV advection along the jet axis [maximum value of 8 potential vorticity units (PVU; 1 PVU = 10^{-6} K m^2 kg^{-1} s^{-1}) day^{-1}; Fig. 8a]. Negative PV advection by the irrotational wind continues between $T - 12$ and $T - 0$ h and contributes to increases in the PV gradient along the jet streak (Figs. 8a,b). During this 12-h period, the jet streak strengthens and remains stationary (Figs. 5a,c), and ascent becomes maximized over the PRE beneath the equatorward jet entrance region (Figs. 8a,b).

Between $T - 0$ and $T + 12$ h, ascent and diabatic outflow intensify (Figs. 8b,c) beneath the equatorward jet entrance region in association with the developing PRE (Figs. 5c,e). The diabatic outflow of the TC is relatively weak and does not appear to affect the jet streak during this time period. Concurrently, a plume of low-PV air (PV values <0.5 PVU) develops over the region of ascent, possibly reflecting a nonconservative reduction of PV due to latent heat release, and extends

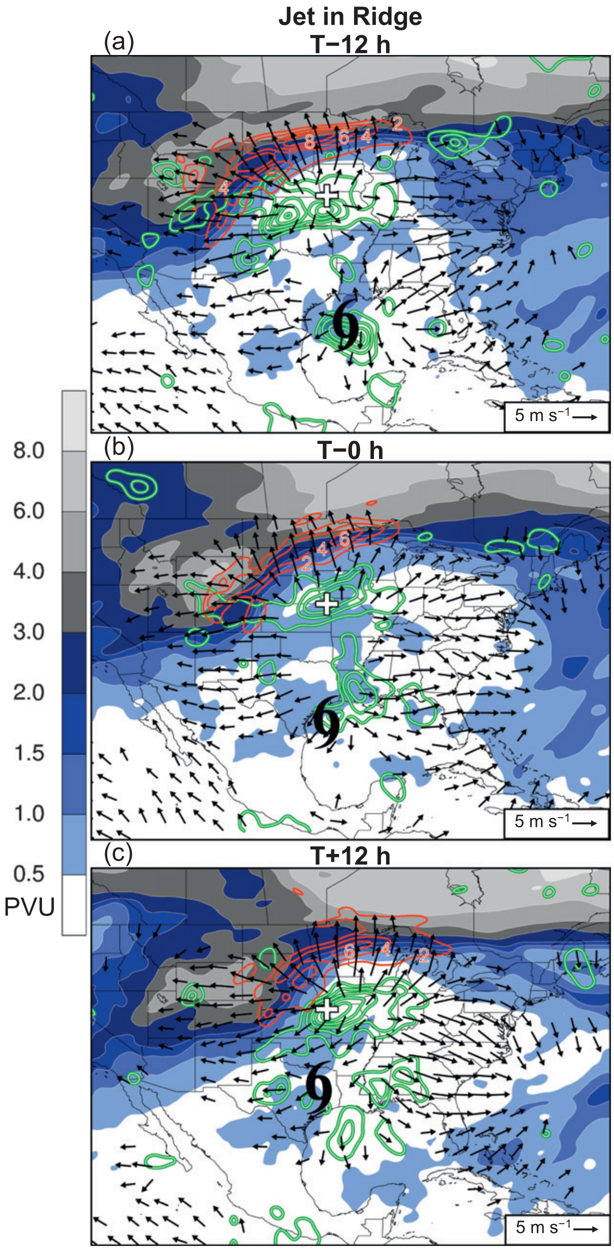

FIG. 8. PRE-relative composites for the seven JR category PREs showing 250–200-hPa layer-averaged irrotational wind (plotted for irrotational wind speeds $\geq$2.5 m s^{-1}, reference vector shown at the bottom right of each panel), 700–500-hPa layer-averaged ascent (contoured in green every 1×10^{-3} hPa s^{-1} starting at -1×10^{-3} hPa s^{-1}), PV in the 250–200-hPa layer (shaded in PVU according to the color bar), and PV advection by the irrotational wind in the 250–200-hPa layer (negative values contoured in red every 2 PVU day^{-1} starting at -2 PVU day^{-1}) at (a) $T - 12$, (b) $T - 0$, and (c) $T + 12$ h. The PRE initiation location and the composite TC location are indicated as in Fig. 5.

poleward into the jet entrance region (Figs. 8b,c). Negative PV advection by the irrotational wind (maximum value of 6 PVU day^{-1}) is concentrated in the jet entrance region, contributing to the maintenance of a large PV gradient and strong wind speeds therein (Figs. 5c,e and 8b,c). Accordingly, the jet entrance region remains approximately stationary poleward of the PRE region between $T - 0$ and $T + 12$ h (Figs. 5c,e).

b. SJ category

1) SYNOPTIC EVOLUTION

Between $T - 12$ and $T + 12$ h, an eastward-moving 200-hPa trough approaches a quasi-stationary 200-hPa ridge extending northeastward from the composite TC and the PRE, coinciding with the strengthening of a southwesterly 200-hPa jet streak downstream and poleward of the TC from 35 to 50 m s^{-1} (Figs. 9a,c,e). The PRE is situated beneath the equatorward entrance region of this jet streak at $T - 0$ and $T + 12$ h (Figs. 9c,e). The TC moves northeastward toward the PRE region between $T - 12$ and $T + 12$ h and begins to interact with a southeastward-moving low-level baroclinic zone (Figs. 10a,c,e). During this interaction, a 7.5–10 m s^{-1} southeasterly LLJ on the eastern flank of the TC circulation impinges upon the baroclinic zone, resulting in warm advection and frontogenesis in the PRE region (Figs. 10a,c,e). An inverted SLP trough develops along the baroclinic zone northeast of the TC center between $T - 0$ and $T + 12$ h (Figs. 9d,f), a signature of a developing warm front. From $T - 12$ to $T + 12$ h, southeasterly 925-hPa water vapor flux is in place on the eastern flank of the TC (Figs. 10b,d,f), and moist air, with PW values >45 mm (Figs. 9b,d,f) and 925-hPa q_v values >14 g kg^{-1} (Figs. 10b,d,f), progresses poleward from the TC into the PRE region. Water vapor flux convergence at 925-hPa develops concurrently with the 925-hPa frontogenesis across the PRE region (Figs. 10c–f). At $T - 0$ and $T + 12$ h, the frontogenesis and water vapor flux convergence in the vicinity of the PRE are notably weaker than in the JR composites (Figs. 6c–f), differences that could partially account for the generally lower maximum rainfall totals observed for the SJ category relative to the JR category (Fig. 4b).

A north–south composite vertical cross section through the PRE at $T - 0$ h (Fig. 11) displays a similar configuration to that of the JR category (Fig. 7), with the LLJ and an associated plume of water vapor extending poleward on the eastern flank of the TC and intersecting the low-level baroclinic zone. Ascent occurs over the low-level baroclinic zone in the presence of

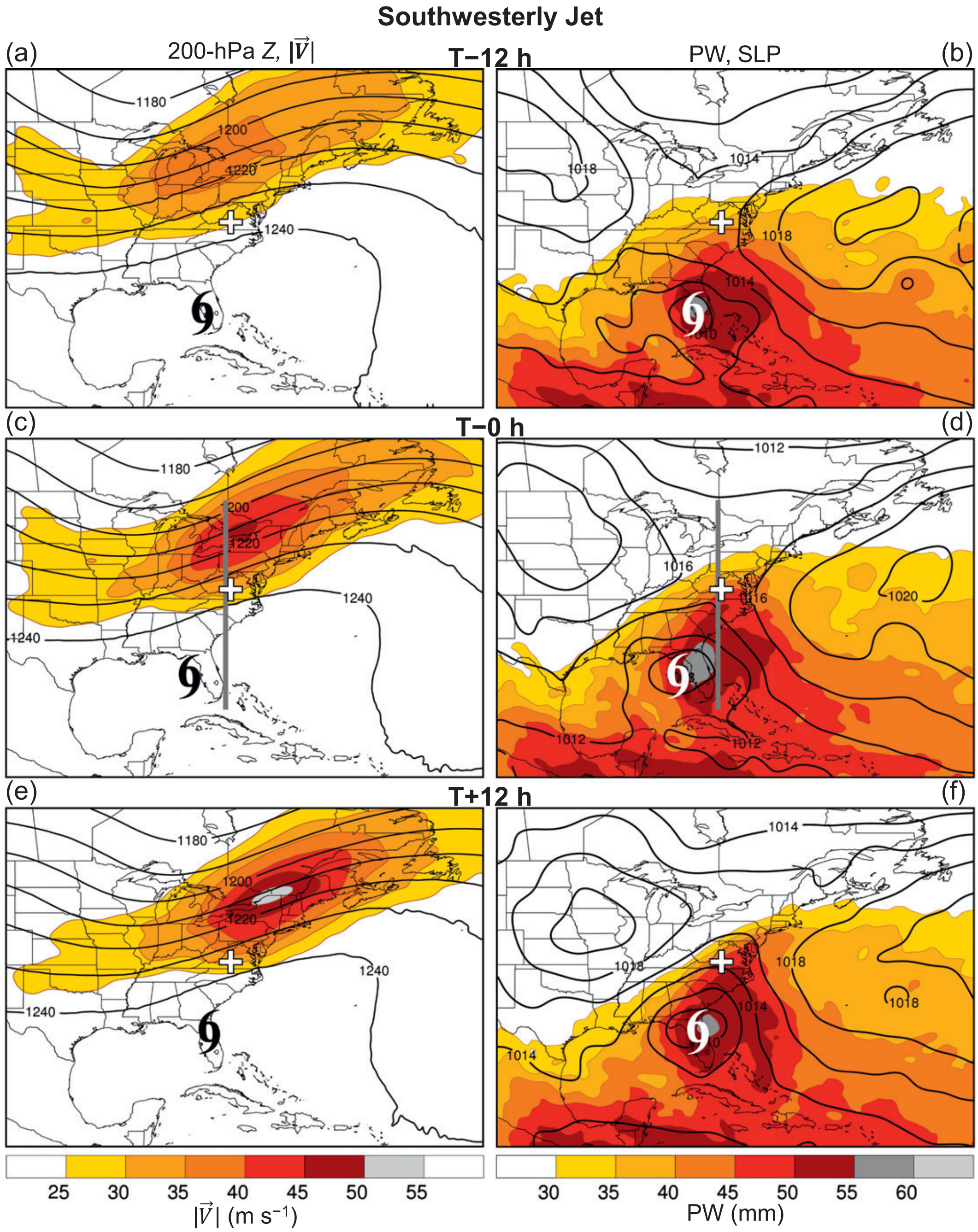

FIG. 9. As in Fig. 5, but for the 17 SJ category PREs. The gray lines in (c),(d) mark the location of the vertical cross section in Fig. 11.

low-level frontogenesis and extends up to ~350 hPa along a region of mid and upper-level frontogenesis (Fig. 11) beneath the entrance region of the 200-hPa jet streak (Fig. 9c). Despite the similarities between the JR and SJ cross sections, the frontogenesis and ascent in the vicinity of the PRE are generally weaker in the SJ cross section.

2) DIABATIC INFLUENCES ON THE UPPER-LEVEL JET

Between $T - 12$ h and $T + 12$ h, an area of high 250–200-hPa PV air approaches the PRE region from the west while low-PV air is advected poleward in connection with 250–200-hPa irrotational winds directed

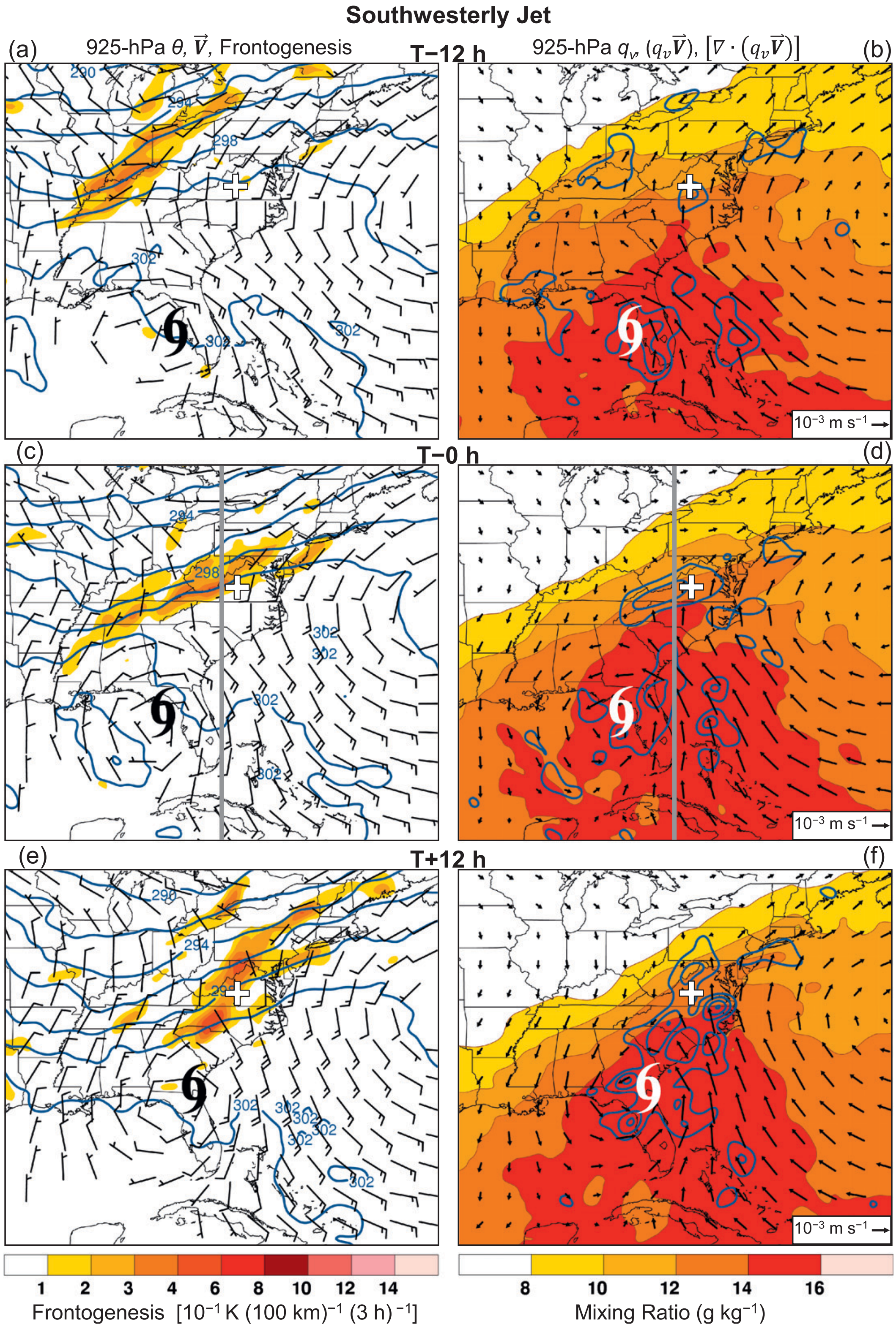

FIG. 10. As in Fig. 6, but for the 17 SJ category PREs. The gray lines in (c),(d) mark the location of the vertical cross section in Fig. 11.

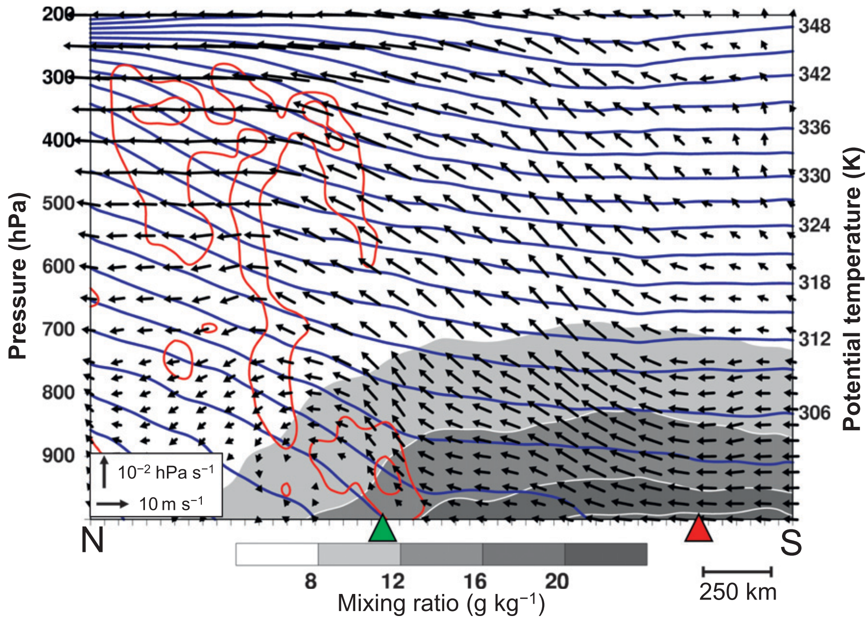

FIG. 11. As in Fig. 7, but for the 17 SJ category PREs along the gray lines in Figs. 9c,d and 10c,d.

outward from an expanding region of 700–500-hPa ascent associated with the TC and the developing PRE (Figs. 12a–c). The PV gradient between the areas of high- and low-PV air increases (Figs. 12a–c), and the jet streak intensifies during the 24-h period (Figs. 9a,c,e). Between $T - 0$ and $T + 12$ h, the irrotational winds linked to the diabatic outflow of both the TC and the PRE are directed into the jet entrance region toward larger values of PV, yielding negative PV advection by the irrotational wind (maximum value reaching 6 PVU day^{-1}) therein (Figs. 12b,c). Concurrently, the PV gradient and wind speeds increase in the jet entrance region, the jet entrance region is effectively anchored poleward of the PRE, and ascent is maintained across the PRE region (Figs. 9c,e and 12b,c). This situation at $T - 0$ and $T + 12$ h differs from that of the JR category (Figs. 8c,d) in that here the outflow of the TC is sufficiently strong and expansive to influence the jet streak.

c. DC category

1) Synoptic evolution

Between $T - 12$ and $T - 0$ h, a positively tilted 200-hPa trough approaches a quasi-stationary ridge extending northeastward from the composite TC and exhibits a trough fracture (e.g., Dean and Bosart 1996; Bosart et al. 2000), whereby the equatorward portion of the trough lags behind the more progressive poleward portion (Figs. 13a,c). Two separate 200-hPa trough axes are evident by $T - 0$ h: one immediately upstream of the TC and the other downstream and poleward of the TC (Fig. 13c). By $T - 0$ h, a 40 m s^{-1} 200-hPa jet streak is situated within a region of confluence between the downstream trough and the ridge (Fig. 13c). As the downstream trough progresses eastward between $T - 0$ and $T + 12$ h, the jet streak strengthens to 45 m s^{-1}, and the equatorward jet entrance region remains positioned over the PRE region (Figs. 13c,e).

A zonally oriented low-level baroclinic zone trailing a surface cyclone positioned in the northeastern portion of the composite domain progresses slowly southeastward into the PRE region between $T - 12$ and $T + 12$ h as a surface anticyclone develops to the northwest of the PRE region beneath the poleward entrance region of the 200-hPa jet streak (Figs. 13b,d,f and 14a,c,e). Concurrently, the cyclonic circulation of the TC moves poleward, and a 7.5–10 m s^{-1} southerly/southeasterly LLJ on the eastern flank of the TC circulation extends into the PRE region (Figs. 14a,c,e). Between $T - 12$ and $T + 12$ h, as in the SJ composites, the LLJ supports poleward water vapor flux on the eastern flank of the TC (Figs. 14b,d,f), and by $T + 12$ h moist conditions, featuring PW values >45 mm (Figs. 13b,d,f) and 925-hPa q_v values >14 g kg^{-1} (Figs. 14b,d,f), are in place in the PRE region.

At $T - 0$ h, in contrast to the JR (Fig. 6c) and SJ categories (Fig. 10c), the PRE is located on the warm side of the baroclinic zone and an associated band of 925-hPa frontogenesis, and does not appear to initially involve a strong interaction between the LLJ and the baroclinic zone (Fig. 14c). Accordingly, a north–south composite vertical cross section through the PRE at $T - 0$ h (Fig. 15) shows ascent occurring on the warm

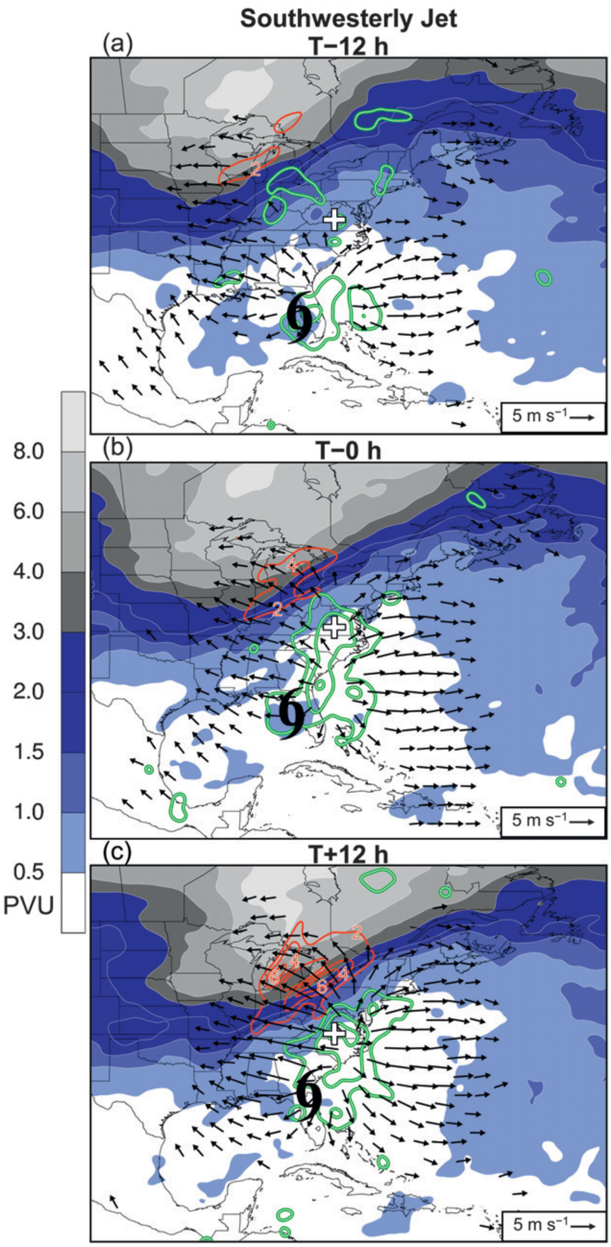

FIG. 12. As in Fig. 8, but for the 17 SJ category PREs.

side of the low-level baroclinic zone at the poleward terminus of the LLJ and an attendant water vapor plume. Ascent extends up to ~300 hPa in the presence of upper-level (~500–200 hPa) frontogenesis (Fig. 15) beneath the equatorward entrance region of the 200-hPa jet streak (Fig. 13c). The frontogenesis and ascent signatures depicted in Fig. 15 near the PRE are comparable in strength to those of the SJ category (Fig. 11) but are weaker than those of the JR category (Fig. 7).

By $T + 12$ h, the TC has moved poleward, and a region of cool air at 925 hPa and an associated SLP ridge have developed across the PRE region, coinciding with the establishment of 925-hPa frontogenesis across the PRE region (Figs. 13f and 14e). The development of the region of cool air and the SLP ridge across the PRE region is possibly a signature of cold-air damming to the east of the Appalachian Mountains (e.g., Bell and Bosart 1988; recall from Fig. 3d that 5 of 10 DC PREs developed east of the Appalachians), a process that can help focus heavy rainfall associated with landfalling TCs in the eastern United States (e.g., Bosart and Dean 1991; Atallah and Bosart 2003; Srock and Bosart 2009).

2) DIABATIC INFLUENCES ON THE UPPER-LEVEL JET

Between $T - 12$ and $T + 12$ h, an area of high 250–200-hPa PV air progresses downstream of the TC, while a persistent plume of low-PV air extends poleward from a region of strengthening 700–500-hPa ascent associated with the TC and the PRE (Figs. 16a–c). The 200-hPa jet streak strengthens (Figs. 13a,c,e) in conjunction with an increase in the PV gradient between the areas of high- and low-PV air (Figs. 16a–c) and remains nearly stationary. From $T - 0$ to $T + 12$ h, as is evident for the SJ category, 250–200-hPa irrotational winds associated with the combined diabatic outflow from the TC and the PRE are directed into the jet entrance region toward larger values of PV, yielding negative PV advection by the irrotational wind (values reaching 6 PVU day^{-1}) therein. Negative PV advection by the irrotational wind is associated with the maintenance of a large PV gradient (Figs. 16b,c) and strong wind speeds in the jet entrance region poleward of the PRE (Figs. 13c,e). The jet entrance region remains stationary between $T - 0$ and $T + 12$ h (Figs. 13c,e), and strong ascent is maintained over the PRE (Figs. 16b,c).

5. Illustrative case studies

Brief case studies of the PREs associated with TC Rita (2005; Fig. 17), TC Wilma (2005; Fig. 18), and TC Ernesto (2006; Fig. 19) are presented here as examples for the JR, SJ, and DC categories, respectively. These example case studies serve to further illustrate the key factors displayed in the composites, as well as to highlight additional details of PRE environments that are not captured in the composites. Synoptic-scale analyses for each case are presented for the 6-h analysis time closest to $T - 0$ h.

a. JR category: TC Rita (2005)

The PRE associated with TC Rita was manifested as a slow-moving ''training line/adjoining stratiform'' MCS (Schumacher and Johnson 2005) that produced maximum rainfall amounts of ~200 mm and caused localized

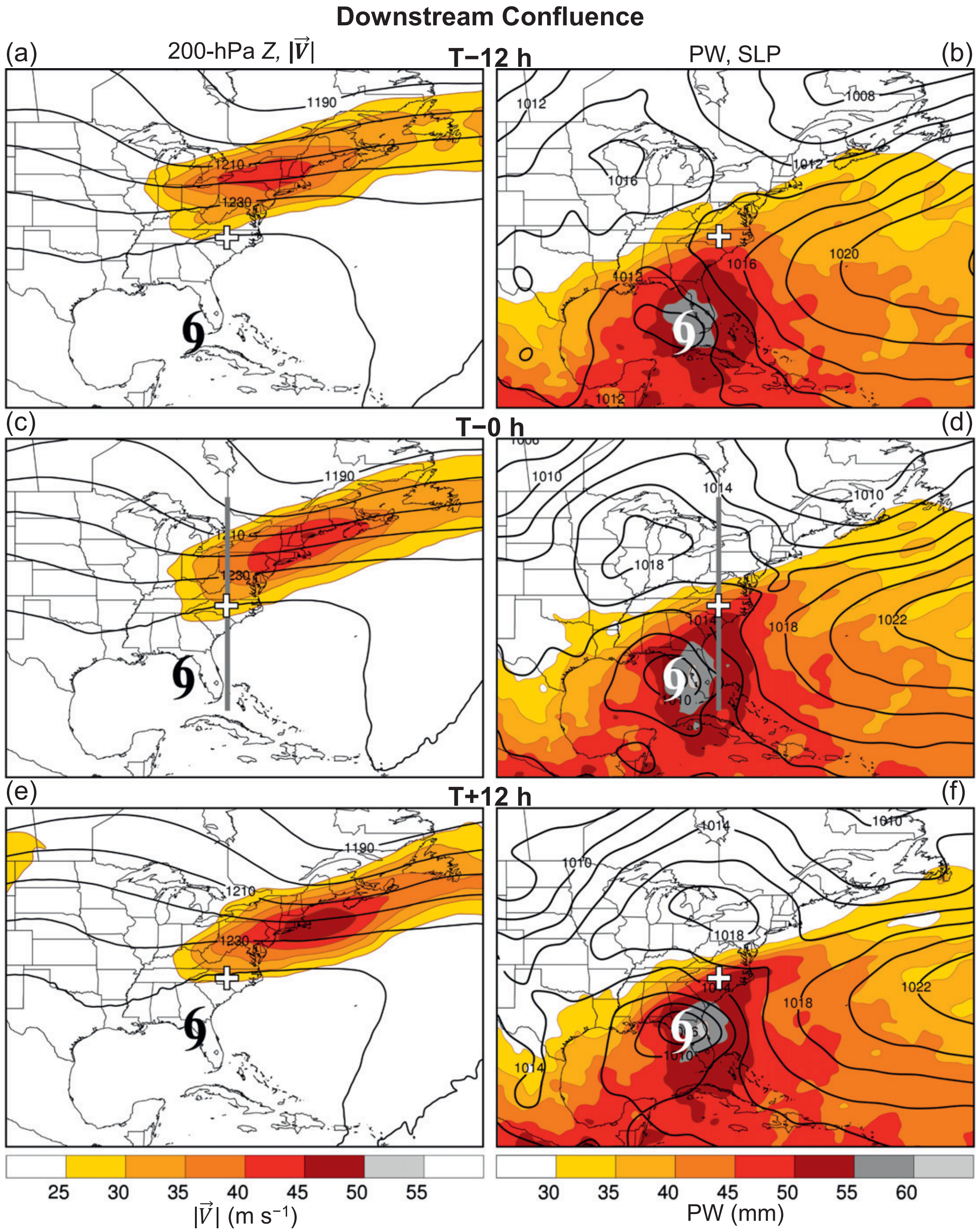

FIG. 13. As in Fig. 5, but for the 10 DC category PREs. The gray lines in (c),(d) mark the location of the vertical cross section in Fig. 15.

flooding over southern Minnesota during 24–25 September 2005. At 0000 UTC 25 September, the developing PRE was located ~1150 km poleward of TC Rita beneath the entrance region of a relatively broad 200-hPa jet streak, which formed from the apparent merger of a polar jet streak with the outflow jet associated with TC Rita (Fig. 17a). During the subsequent 12 h (not shown), the PRE matured beneath the equatorward entrance region of the polar jet streak, which strengthened during this time period. The PRE developed on the cool side of a quasi-stationary low-level baroclinic zone in the presence of deep vigorous ascent linked to warm advection and frontogenesis at the terminus of a southeasterly LLJ (Figs. 17c,d). Frontogenesis was maximized west of the

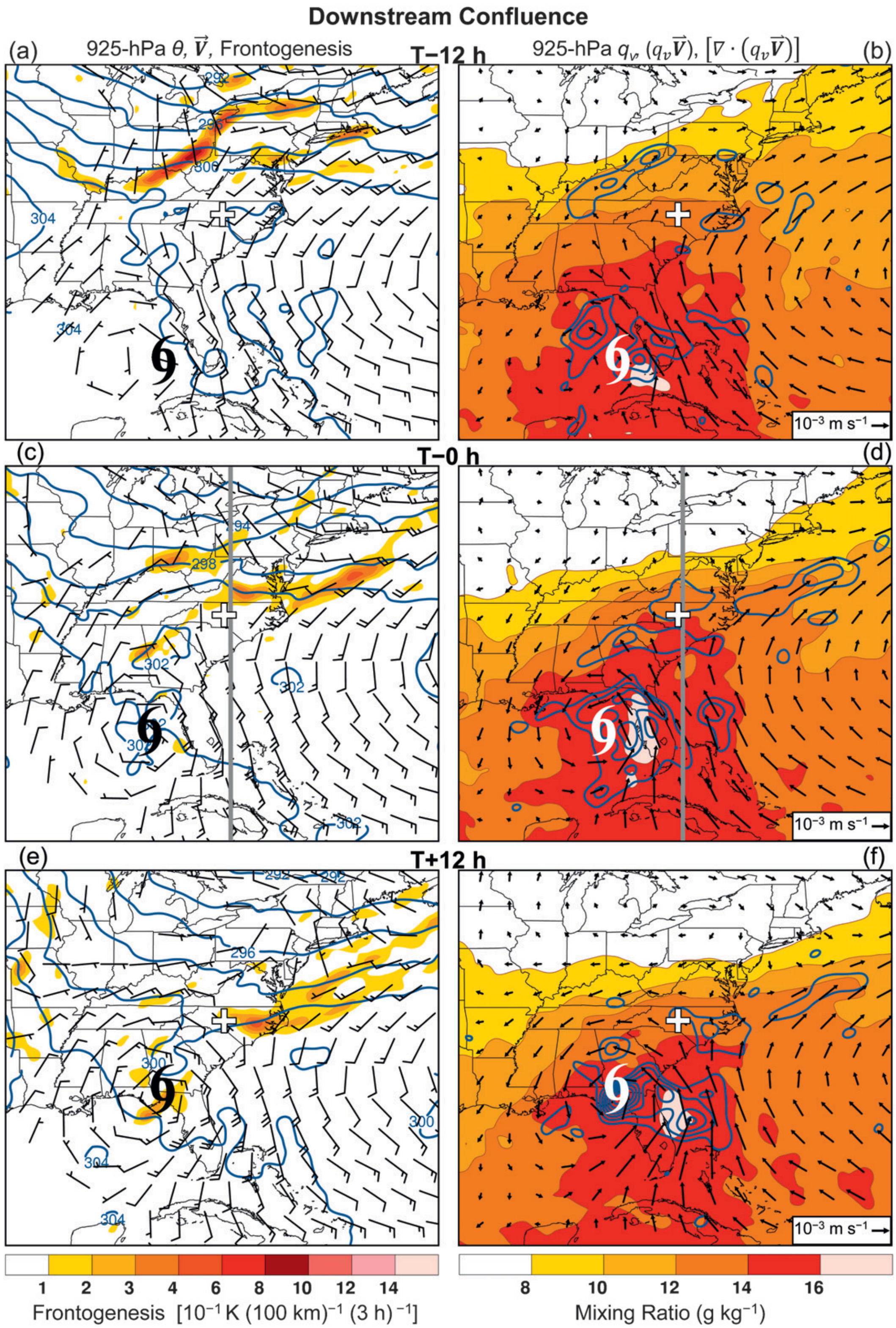

FIG. 14. As in Fig. 6, but for the 10 DC category PREs. The gray lines in (c),(d) mark the location of the vertical cross section in Fig. 15.

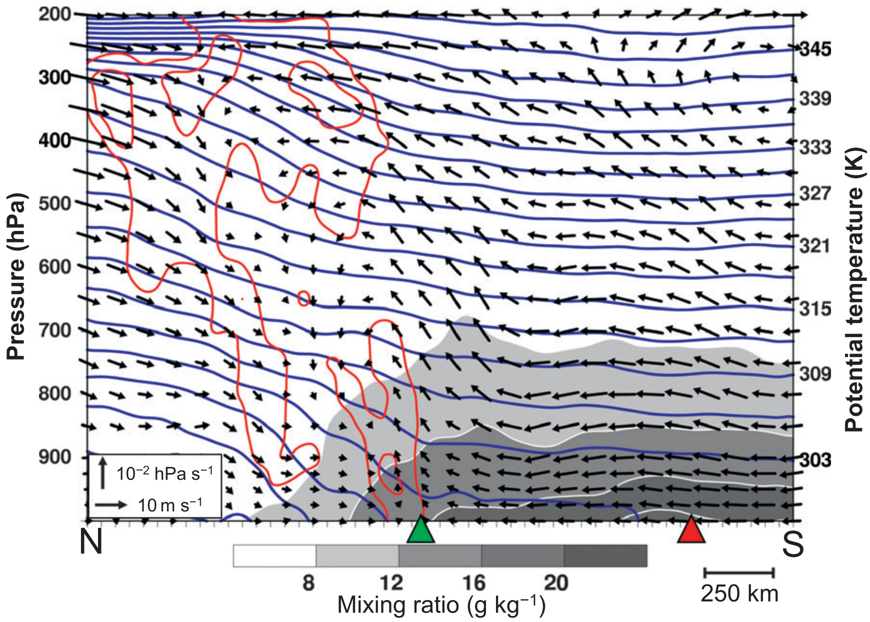

FIG. 15. As in Fig. 7, but for the 10 DC category PREs along the gray lines in Figs. 13c,d and 14c,d.

PRE on the equatorward edge of a cold surge east of the Rocky Mountains (Fig. 17c). The LLJ extended poleward from the TC Rita circulation between a weak surface cyclone over the central plains and a surface anticyclone over the eastern United States (Figs. 17b,c). The PRE was positioned within a band of relatively large water vapor content (PW values of 35–45 mm; Fig. 17b), which is visibly separate in the PW field from the water vapor plume associated with TC Rita. Despite this apparent separation in the PW field, water vapor transport from the northern flank of the TC into the PRE region occurred at low levels (i.e., below 700 hPa; not shown), a process that is consistent with the configuration of the LLJ poleward of TC Rita (Figs. 4c,d). As the PRE intensified and matured between 0000 and 1200 UTC 25 September (not shown), the LLJ strengthened, and a plume of water vapor with PW values of 30–40 mm extending poleward from TC Rita merged with the band of water vapor over the PRE region.

b. SJ category: TC Wilma (2005)

The PRE associated with TC Wilma occurred during 23–25 October 2005 along the southeastern U.S. coast as the TC moved poleward across the Caribbean Sea and the eastern Gulf of Mexico. This PRE is not particularly notable for producing large amounts of rainfall over land (most of the rainfall occurred just offshore), but rather for the robust dynamical interaction between TC Wilma and a strongly baroclinic synoptic-scale environment that was associated with PRE development. At 1800 UTC 23 October, the developing PRE was manifested as a band of heavy rainfall located off the southeastern U.S. coast beneath the equatorward entrance region of a strong southwesterly 200-hPa jet streak that was positioned downstream of a deep upper-level trough over the Great Lakes (Figs. 18a,c). The PRE developed in the presence of low- and midlevel frontogenesis as a southerly LLJ on the eastern flank of the TC Wilma circulation impinged upon a baroclinic zone trailing to the southwest of a midlatitude cyclone off the coast of Nova Scotia (Figs. 18b–d). This frontogenesis was associated with a thermally direct circulation centered near 750 hPa beneath the upper-level jet entrance region, with the PRE positioned in the ascending branch of the circulation (Fig. 18d). A broad plume of moist air (PW values of 45–60 mm; Fig. 18b) extended northeastward from TC Wilma into the region of ascent in connection with strong water vapor transport by the LLJ (Fig. 18d).

c. DC category: TC Ernesto (2006)

The PRE associated with TC Ernesto was manifested as a quasi-stationary mesoscale region of convective and stratiform precipitation, producing maximum rainfall amounts of ~100 mm during 30–31 August 2006 over North Carolina and Virginia. This PRE is notable because it occurred along the eventual track of TC Ernesto. The PRE and TC Ernesto together produced a broad area of rainfall amounts exceeding 125 mm (local maxima of >250 mm) across North Carolina and

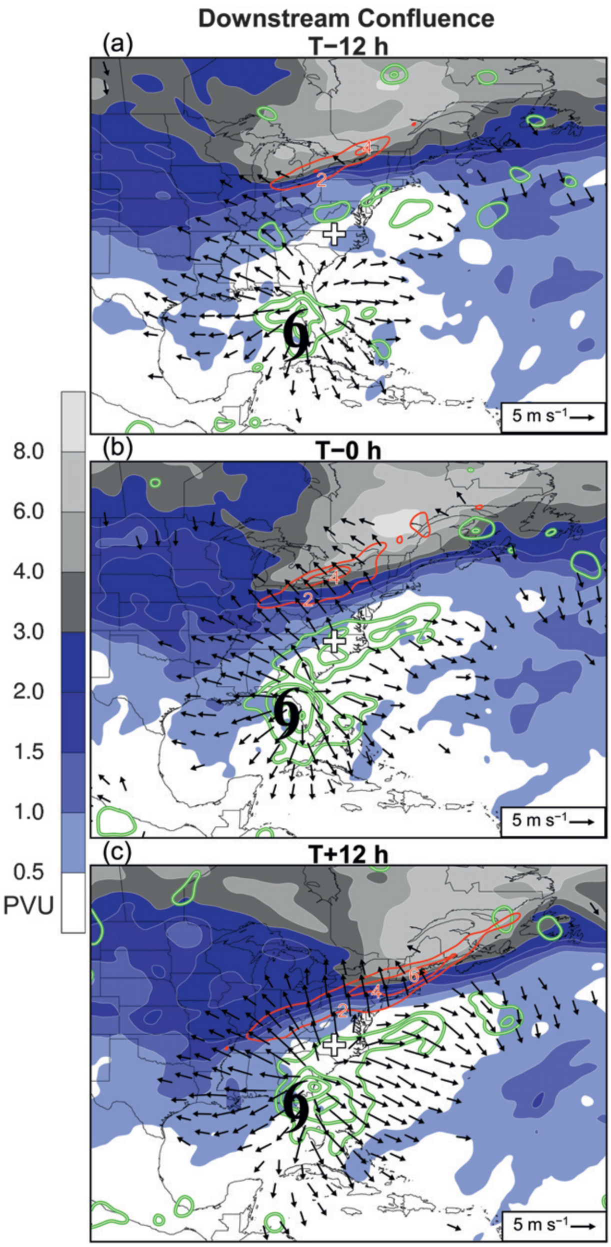

FIG. 16. As in Fig. 8, but for the 10 DC category PREs.

Virginia during 30 August–1 September, leading to river flooding at some locations (Franklin and Brown 2008). At 1800 UTC 30 August, the developing PRE was located beneath the equatorward entrance region of a 200-hPa jet streak, which was situated in a region of confluence between a downstream trough and a quasi-stationary ridge poleward of TC Ernesto (Fig. 19a). Convection associated with the PRE was initiated near a region of cold-air damming in the presence of deep ascent overlying a region of low-level confluence at the terminus of a southerly LLJ located on the eastern flank of the TC Ernesto circulation (Figs. 19c,d). During the subsequent 12 h (not shown), the PRE intensified and matured as the region of cold-air damming expanded southward, forcing low-level ascent and triggering new convection across North Carolina. The PRE was located within a band of large water vapor content (PW values >55 mm; Fig. 19b) established in connection with water vapor transported poleward from the eastern/northeastern flank of TC Ernesto (Fig. 19d) and from the northern Gulf of Mexico (not shown).

6. Synthesis and conclusions

In this paper, the synoptic-scale environments of PREs occurring to the east of the Rocky Mountains during 1988–2010 in association with Atlantic basin TCs were examined through composite analysis and brief case studies. Three categories (i.e., JR, SJ, and DC) were identified by subjectively classifying PREs according to the synoptic-scale upper-level flow configuration within which they developed. In contrast to GBS10, who classified PREs according to jet streak curvature, the classification procedure in the current study focused on the structure of the upper-level jet streak and its location relative to key flow features such as upper-level troughs and ridges and the TC. By classifying PREs in this way, the composites in the current study display key details that are otherwise obscured when composites are generated solely on the basis of jet streak curvature.

Despite the differences in PRE classification between the current study and GBS10, the composites for the JR, SJ, and DC categories capture many of the key characteristics elucidated by GBS10 in their composites of PREs, which consisted only of PREs in their ''anticyclonically curved'' category. Specifically, the composites in the current study demonstrate that PREs tend to form as moist air is transported poleward from a TC and is forced to ascend near a low-level baroclinic zone and beneath the equatorward entrance region of an upper-level jet streak. The composites also indicate that the upper-level diabatically driven outflow from the PRE and/or the TC can interact with the upper-level jet streak, helping to strengthen the jet streak and reinforce ascent over the PRE region. Consistent with this result, GBS10 showed in their composites that the diabatic outflow of a TC can contribute to jet streak intensification prior to PRE development, while Bosart et al. (2012) documented a robust interaction between the diabatic outflow of three consecutive PREs and a subtropical jet streak.

Although the composites for the three categories share common signatures, each category features a characteristic phasing of a TC with the synoptic-scale flow pattern into

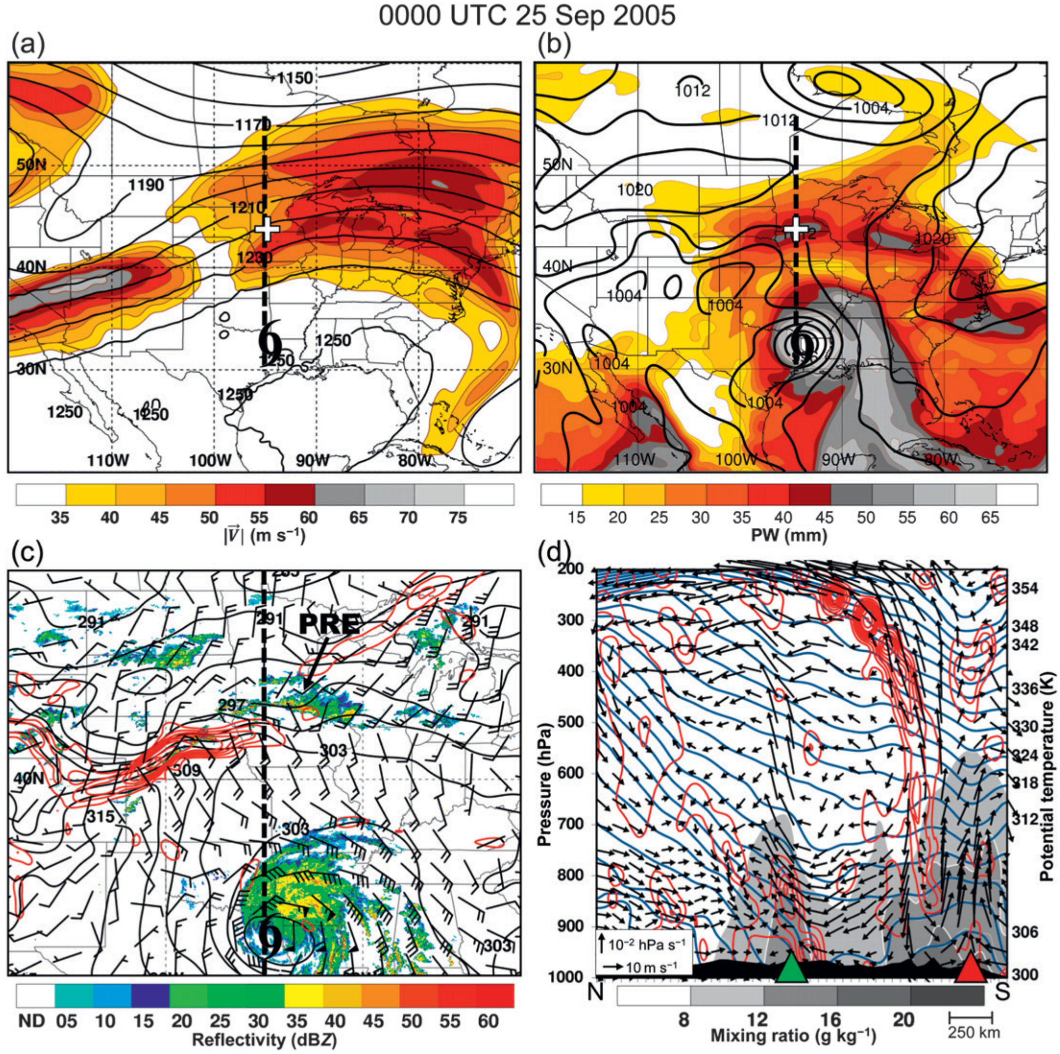

FIG. 17. Synoptic-scale analyses for the PRE associated with TC Rita at 0000 UTC 25 Sep 2005 showing (a) 200-hPa geopotential height (contoured in black every 10 dam) and wind speed (shaded in m s^{-1} according to the color bar); (b) SLP (contoured in black every 2 hPa) and PW (shaded in mm according to the color bar); (c) WSI National Operational Weather Radar (NOWrad) radar reflectivity (shaded in dBZ according to the color bar), 925-hPa potential temperature (contoured in black every 3 K), wind (plotted for wind speeds $\geq$7.5 m s^{-1}, half barb: 2.5 m s^{-1}; full barb: 5 m s^{-1}), and Petterssen frontogenesis [contoured in red every 2 K (100 km)$^{-1}$ (3 h)$^{-1}$ starting at 1 K (100 km)$^{-1}$ (3 h)$^{-1}$]; and (d) vertical cross section along the dashed black lines in (a)–(c) displaying potential temperature (contoured in blue every 3 K), Petterssen frontogenesis [contoured in red every 2 $\times$ 10^{-1} K (100 km)$^{-1}$ (3 h)$^{-1}$ starting at 1 $\times$ 10^{-1} K (100 km)$^{-1}$ (3 h)$^{-1}$], water vapor mixing ratio (shaded in g kg^{-1} according to the grayscale bar), and flow vectors in the plane of the cross section (horizontal component in m s^{-1} and vertical component in hPa s^{-1}; reference vectors shown in lower left). The PRE location in (a),(b) is indicated by the "+" symbol, and the TC location in (a)–(c) is indicated by the tropical storm symbol. The latitudinal positions of the PRE and the TC in (d) are indicated by the green and red triangles, respectively.

which the TC moves and therefore represents a unique pathway to PRE development. The distinguishing characteristics of each PRE category are illustrated schematically in Fig. 20. For the JR category (Fig. 20a), the TC moves beneath a broad upper-level ridge typically positioned over the central United States, the circulation of the TC links with a poleward-extending LLJ, and moist airstreams poleward from the eastern flank of the TC to a distant region (median separation distance of 1120 km) of frontogenetically forced ascent. The JR PREs are commonly manifested as quasi-stationary MCSs, typically involving stronger frontogenesis and producing significantly larger maximum rainfall totals than SJ and DC PREs. Two recently studied PREs

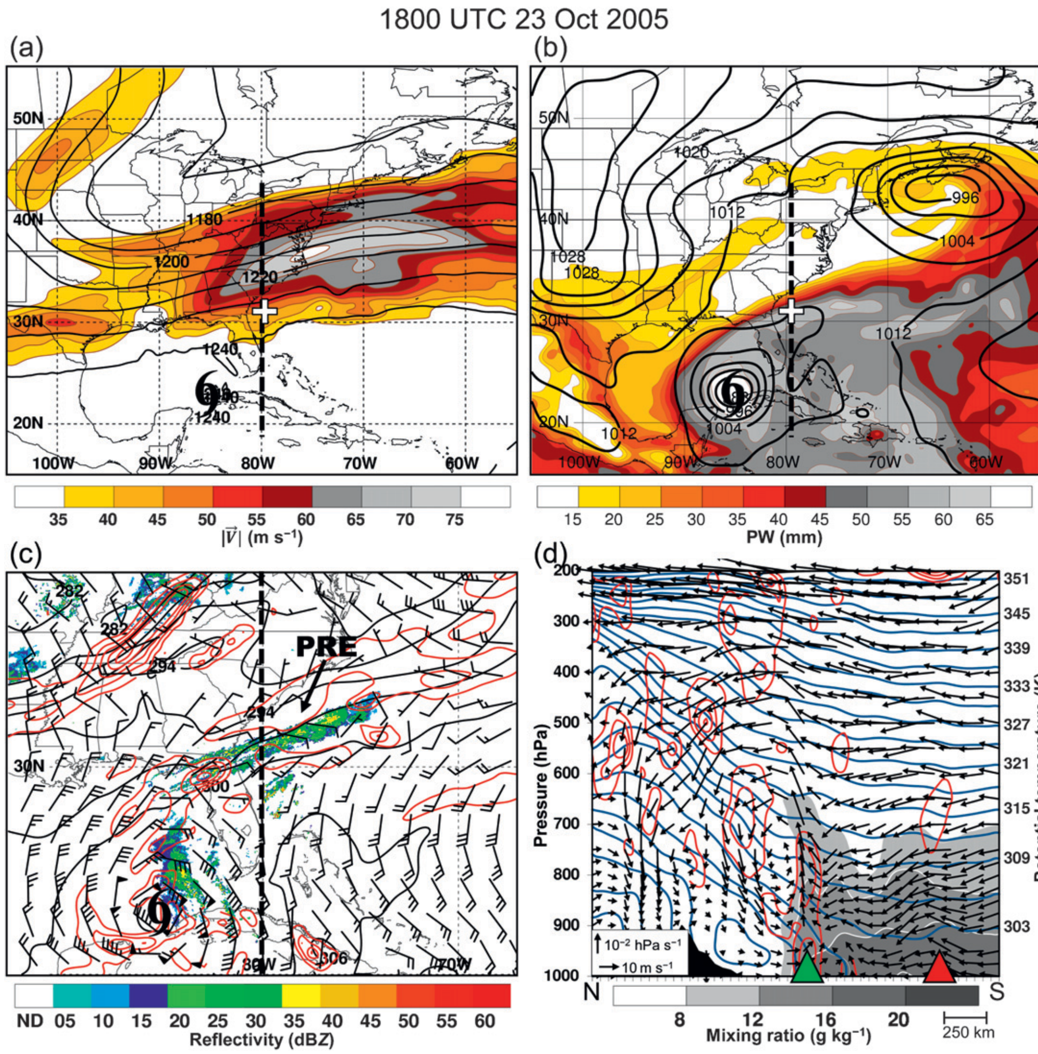

FIG. 18. As in Fig. 17, but at 1800 UTC 23 Oct 2005 for the PRE associated with TC Wilma.

associated with TC Erin (2007; GBS10; Schumacher et al. 2011; Schumacher and Galarneau 2012) and TC Ike (2008; Bosart et al. 2012; Schumacher and Galarneau 2012), respectively, serve as illustrative examples of high-impact JR PREs.

The SJ category (Fig. 20b) features an interaction between the TC and an upstream midlatitude trough and an associated baroclinic zone. In contrast to the JR category, the TC circulation directly facilitates poleward water vapor transport into the PRE region and helps to drive warm advection and frontogenesis along the baroclinic zone. At upper levels, as the upstream trough approaches a quasi-stationary ridge linked to the diabatic outflow of the TC and the PRE, a southwesterly jet streak intensifies downstream and poleward of the PRE, placing the PRE in an area of strong ascent beneath equatorward jet entrance region. Interestingly, the flow pattern associated with the SJ category bears resemblance to the initial stages of ET (e.g., Klein et al. 2000).

For the DC category (Fig. 20c), a trough progresses downstream and poleward of the TC and a slow-moving baroclinic zone trails behind it. As in the SJ category, the TC circulation facilitates poleward water vapor transport into the PRE region. However, in contrast to SJ PREs, DC PREs often do not initially involve a strong interaction between the TC circulation and the baroclinic zone. Rather, DC PREs commonly (but not always) develop on the warm side of the baroclinic zone and an associated region of frontogenesis, often relying on mesoscale boundaries or orographic features that are not well resolved in synoptic-scale composites for focusing low-level ascent and initiating heavy rainfall. Mesoscale boundaries can be established in conjunction with cold-air damming east of the Appalachians along

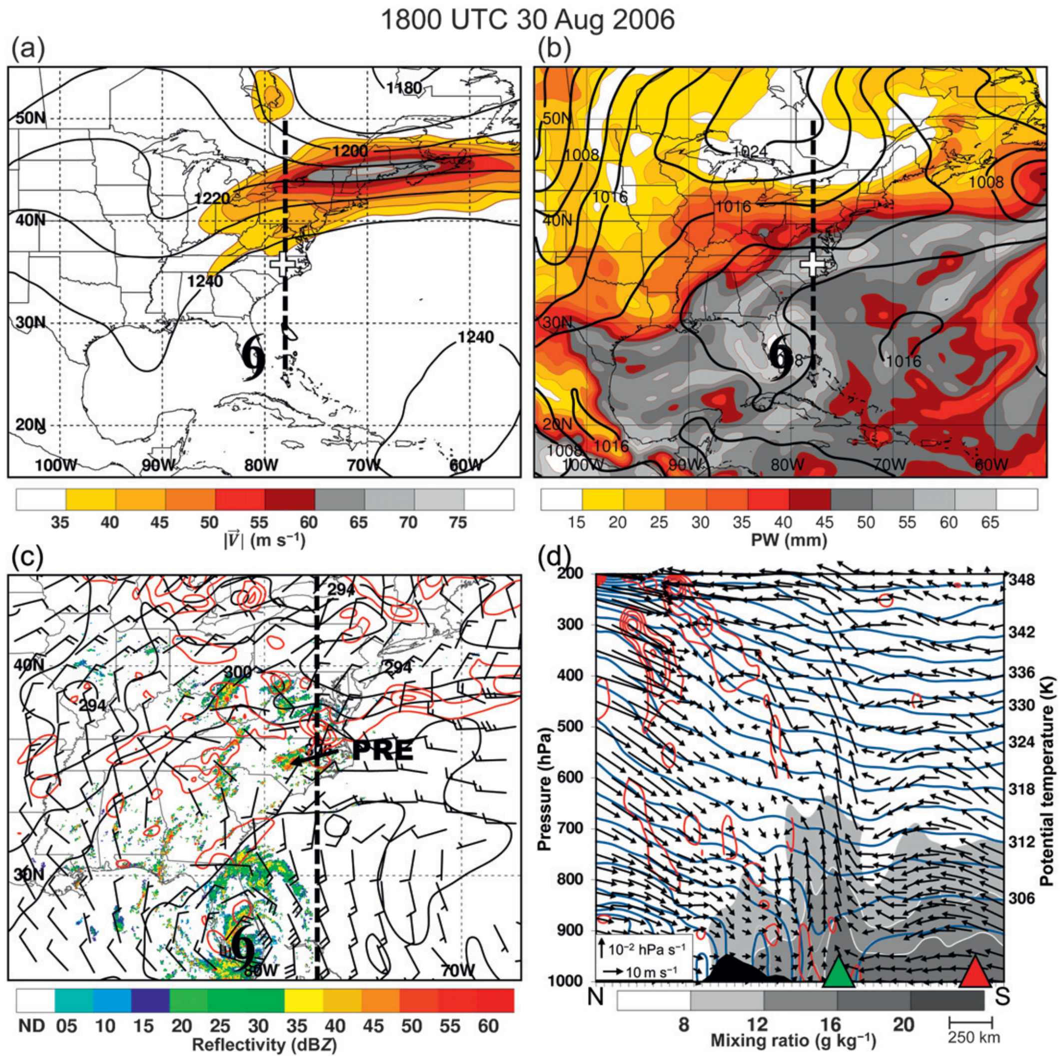

FIG. 19. As in Fig. 17, but at 1800 UTC 30 Aug 2006 for the PRE associated with TC Ernesto.

the trailing baroclinic zone, coastal frontogenesis, frictional convergence, or evaporative cooling associated with the PRE. At upper levels, a similar interaction to that associated with the SJ category occurs between the combined diabatic outflow of the TC and the PRE and a jet streak. A key difference, however, between the SJ and DC categories is that the trough associated with the jet streak is positioned downstream and poleward, rather than upstream, of the TC for the DC category.

A benefit of the classification procedure used in the current study is that it allows for a qualitative assessment of the influences of a TC in producing a PRE. Numerical model-based experiments would be required to quantify these influences and are a possible avenue for future research. It is postulated that the role of a TC in PRE development can be either *direct* or *indirect*, based upon the apparent influence of the TC in 1) supplying water vapor to the PRE region and 2) forcing ascent in the PRE region. A direct role of a TC in PRE development is commonly featured for PREs in the SJ and DC categories. In these categories, strong poleward low-level flow (i.e., an LLJ) associated with the TC circulation facilitates poleward water vapor transport into the PRE region and aids in driving ascent as the low-level flow impinges upon a preexisting baroclinic zone, a mesoscale boundary, or a region of orography. In addition, the diabatic outflow of the TC helps to strengthen an upper-level jet streak downstream and poleward of the PRE and to reinforce ascent over the PRE region. Scenarios featuring a direct role of a TC in PRE development frequently include key factors involved in the ET process (e.g., Jones et al. 2003), pointing to possible, yet unexplored, linkages between PRE development and ET.

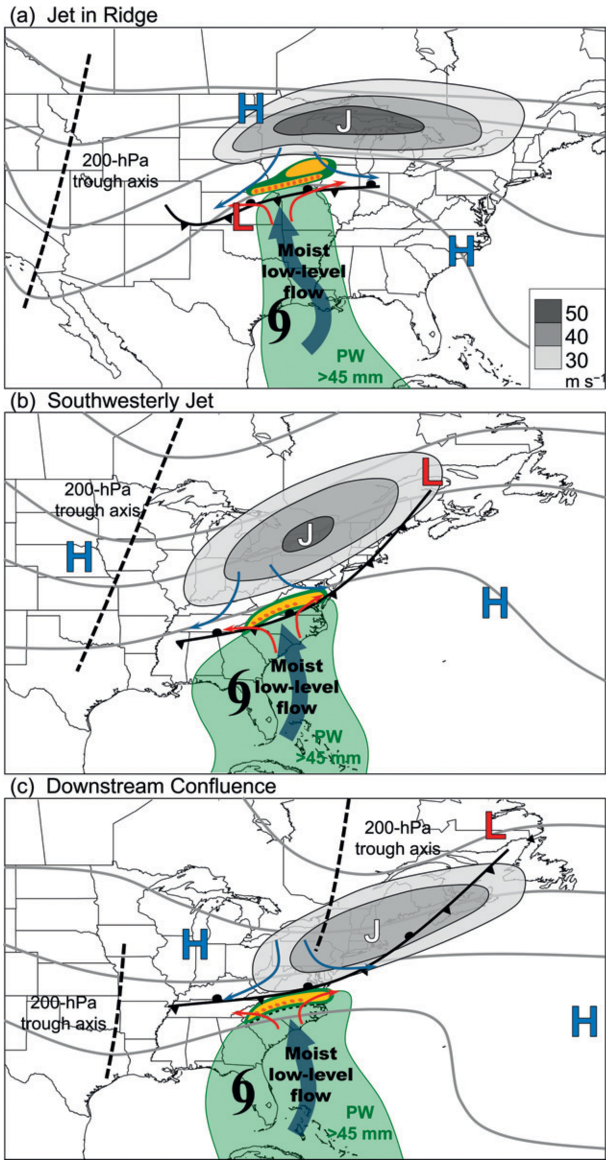

FIG. 20. Conceptual model of the key synoptic-scale features and processes for (a) JR, (b) SJ, and (c) DC category PREs. The gray contours denote the 200-hPa geopotential height field, with the thick dashed black line marking the primary trough axis. The gray shaded regions represent 200-hPa wind speed [m s^{-1}; gray shade bar in (a)] and the ''J'' marks the 200-hPa wind speed maximum. The thin red and blue arrows represent 925-hPa streamlines associated with regions of warm and cold advection, respectively. The position of the surface front is shown in standard frontal notation, and the positions of the SLP maxima and minima are marked by the ''H'' and the ''L'' symbols, respectively. The light green shading indicates the region with PW values >45 mm. The thick blue arrow represents a corridor of moist low-level flow. The dark green, gold, and orange shaded regions represent radar reflectivity thresholds of 20, 35, and 50 dB*Z*, respectively, associated with the PRE. The TC location is indicated by the tropical storm symbol.

The JR category, in contrast to the SJ and DC categories, represents a scenario in which a TC plays an indirect role in PRE development, with the TC primarily acting as a source region of water vapor that is ''tapped'' and transported by an LLJ into a distant region of frontogenetically forced ascent. The JR composites indicate that this tapping of water vapor occurs when the TC becomes embedded in a synoptic-scale flow pattern resembling the Maddox et al. (1979) frontal type flash-flood pattern. Typically, as demonstrated in the JR composites, lifting in the vicinity of JR PREs is not directly influenced by the cyclonic circulation or by the upper-level outflow of the TC. This lack of direct influence on the part of the TC can result when the TC circulation and upper-level outflow are relatively weak or small-scale and/or when the TC and PRE are separated by a large distance. As posited by GBS10 for the TC Erin (2007) PRE, it is plausible that for many JR PREs rainfall would occur even in the absence of the TC, but the presence of additional water vapor from the TC serves to enhance rainfall accumulations. Consistent with this interpretation, numerical model simulations of the TC Erin (2007) PRE by Schumacher et al. (2011), in which the moisture plume associated with TC Erin was removed, showed a 25% reduction in area-integrated rainfall and a 50% reduction in the maximum rainfall total for the PRE.

It is acknowledged that PREs are not limited to occurring within the three categories described in the current study. Accordingly, a so-called unclassifiable (UC) category was included, containing events that did not fit into any of the three categories. UC PREs were not examined in the current study and therefore represent a possible avenue for future research. Furthermore, PREs occurring in the United States east of the Rockies in association with Atlantic basin TCs have only been considered here. PREs or PRE-like events can occur in other parts of the world, such as the southwestern United States in association with east Pacific TCs (e.g., Corbosiero et al. 2009) and eastern Asia in association with western North Pacific TCs (e.g., Wang et al. 2009; Meng and Zhang 2012; Byun and Lee 2012), involving other unique synoptic-scale flow patterns. It is also acknowledged that there exist other methods of classification and composite analysis for examining the environments of PREs; we have presented only one possible approach. The results of the PRE classification and composite analysis presented in the current study can help improve identification and prediction of PREs in short- and medium-range forecasts. To supplement these results, future work could include a comprehensive assessment of operational numerical model performance in predicting PREs on short- and medium-range time scales.

Acknowledgments. The authors thank Dr. Thomas Galarneau (NCAR), Jonas Asuma (GL Garrad Hassan), Dr. Jason Cordeira (EarthRisk Technologies), and Dr. Marty Ralph (NOAA/ESRL) for helpful discussions and assistance during this research. Thanks also go to Dr. Russ Schumacher (Colorado State University) and one anonymous reviewer whose comments and suggestions helped to improve the quality of this manuscript. This research was initially conducted as part of the first author's M.S. thesis at the University at Albany, SUNY, which was funded by the NOAA Collaborative Science, Technology, and Applied Research (CSTAR) Program Grant NA07NWS4680001. Additional support during the later stages of this research was provided by the Water Cycle Branch at NOAA/ESRL.

REFERENCES

Agustí-Panareda, A., C. D. Thorncroft, G. C. Craig, and S. L. Gray, 2004: The extratropical transition of Hurricane Irene (1999): A potential vorticity perspective. *Quart. J. Roy. Meteor. Soc.,* **130,** 1047–1074.

Archambault, H. M., 2011: The downstream extratropical flow response to recurving western North Pacific tropical cyclones. Ph.D. dissertation, University at Albany, State University of New York, 212 pp. [Available online at http://www.atmos.albany.edu/student/heathera/dissertation/.]

Atallah, E. H., and L. F. Bosart, 2003: The extratropical transition and precipitation distribution of Hurricane Floyd (1999). *Mon. Wea. Rev.,* **131,** 1063–1081.

——, ——, and A. R. Aiyyer, 2007: Precipitation distribution associated with landfalling tropical cyclones over the eastern United States. *Mon. Wea. Rev.,* **135,** 2185–2206.

Augustine, J. A., and F. Caracena, 1994: Lower-tropospheric precursors to nocturnal MCS development over the central United States. *Wea. Forecasting,* **9,** 116–135.

Bell, G. D., and L. F. Bosart, 1988: Appalachian cold-air damming. *Mon. Wea. Rev.,* **116,** 137–161.

Bosart, L. F., and F. H. Carr, 1978: A case study of excessive rainfall centered around Wellsville, New York, 20–21 June 1972. *Mon. Wea. Rev.,* **106,** 348–362.

——, and D. B. Dean, 1991: The Agnes rainstorm of June 1972: Surface feature evolution culminating in inland storm redevelopment. *Wea. Forecasting,* **6,** 515–537.

——, and G. M. Lackmann, 1995: Postlandfall tropical cyclone reintensification in a weakly baroclinic environment: A case study of Hurricane David (September 1979). *Mon. Wea. Rev.,* **123,** 3268–3291.

——, W. E. Bracken, J. Molinari, C. S. Velden, and P. G. Black, 2000: Environmental influences on the rapid intensification of Hurricane Opal (1995) over the Gulf of Mexico. *Mon. Wea. Rev.,* **128,** 322–352.

——, J. M. Cordeira, T. J. Galarneau Jr., B. J. Moore, and H. M. Archambault, 2012: An analysis of multiple predecessor rain events ahead of Tropical Cyclones Ike and Lowell: 10–15 September 2008. *Mon. Wea. Rev.,* **140,** 1081–1107.

Byun, K.-Y., and T.-Y. Lee, 2012: Remote effects of tropical cyclones on heavy rainfall over the Korean peninsula—Statistical and composite analysis. *Tellus,* **64A,** 14983, doi:10.3402/tellusa.v64i0.14983.

Cammas, J.-P., D. Keyser, G. M. Lackmann, and J. Molinari, 1994: Diabatic redistribution of potential vorticity accompanying the development of an outflow jet within a strong extratropical cyclone. Preprints, *Int. Symp. on the Life Cycles of Extratropical Cyclones,* Vol. II, Bergen, Norway, Geophysical Institute, University of Bergen, 403–409.

Coniglio, M. C., J. Y. Hwang, and D. J. Stensrud, 2010: Environmental factors in the upscale growth and longevity of MCSs derived from Rapid Update Cycle analyses. *Mon. Wea. Rev.,* **138,** 3514–3539.

Corbosiero, K. L., M. J. Dickinson, and L. F. Bosart, 2009: The contribution of eastern North Pacific tropical cyclones to the rainfall climatology of the southwest United States. *Mon. Wea. Rev.,* **137,** 2415–2435.

Cote, M. R., 2007: Predecessor rain events in advance of tropical cyclones. M.S. thesis, Department of Earth and Atmospheric Sciences, University at Albany, State University of New York, 200 pp. [Available online at http://cstar.cestm.albany.edu/CAP_Projects/Project10/index.htm.]

Dean, D. B., and L. F. Bosart, 1996: Northern Hemisphere 500-hPa trough merger and fracture: A climatology and case study. *Mon. Wea. Rev.,* **124,** 2644–2671.

Franklin, J. L., and D. P. Brown, 2008: Atlantic hurricane season of 2006. *Mon. Wea. Rev.,* **136,** 1174–1200.

Fritsch, J. M., and R. E. Carbone, 2004: Improving quantitative precipitation forecasts in the warm season: A USWRP research and development strategy. *Bull. Amer. Meteor. Soc.,* **85,** 955–965.

Galarneau, T. J., Jr., L. F. Bosart, and R. S. Schumacher, 2010: Predecessor rain events ahead of tropical cyclones. *Mon. Wea. Rev.,* **138,** 3272–3297.

Harr, P. A., and R. L. Elsberry, 2000: Extratropical transition of tropical cyclones over the western North Pacific. Part I: Evolution of structural characteristics during the transition process. *Mon. Wea. Rev.,* **128,** 2613–2633.

——, ——, and T. F. Hogan, 2000: Extratropical transition of tropical cyclones over the western North Pacific. Part II: The impact of midlatitude circulation characteristics. *Mon. Wea. Rev.,* **128,** 2634–2653.

Jones, S. C., and Coauthors, 2003: The extratropical transition of tropical cyclones: Forecast challenges, current understanding, and future directions. *Wea. Forecasting,* **18,** 1052–1092.

Junker, N. W., R. S. Schneider, and S. L. Fauver, 1999: A study of heavy rainfall events during the Great Midwest Flood of 1993. *Wea. Forecasting,* **14,** 701–712.

Keyser, D., M. J. Reeder, and R. J. Reed, 1988: A generalization of Petterssen's frontogenesis function and its relation to the forcing of vertical motion. *Mon. Wea. Rev.,* **116,** 762–780.

Klein, P. M., P. A. Harr, and R. L. Elsberry, 2000: Extratropical transition of western North Pacific tropical cyclones: An overview and conceptual model of the transformation stage. *Wea. Forecasting,* **15,** 373–395.

——, ——, and ——, 2002: Extratropical transition of western North Pacific tropical cyclones: Midlatitude and tropical cyclone contributions to reintensification. *Mon. Wea. Rev.,* **130,** 2240–2259.

Maddox, R. A., C. F. Chappell, and L. R. Hoxit, 1979: Synoptic and meso-α scale aspects of flash flood events. *Bull. Amer. Meteor. Soc.,* **60,** 115–123.

Meng, Z., and Y. Zhang, 2012: On the squall lines preceding landfalling tropical cyclones in China. *Mon. Wea. Rev.,* **140,** 445–470.

Moore, J. T., F. H. Glass, C. E. Graves, S. M. Rochette, and M. J. Singer, 2003: The environment of warm-season elevated thunderstorms associated with heavy rainfall over the central United States. *Wea. Forecasting,* **18,** 861–878.

Petterssen, S., 1936: Contribution to the theory of frontogenesis. *Geofys. Publ.,* **11** (6), 1–27.

——, 1956: *Motion and Motion Systems.* Vol. 2, *Weather Analysis and Forecasting,* McGraw-Hill, 428 pp.

Riemer, M., S. C. Jones, and C. A. Davis, 2008: The impact of extratropical transition on the downstream flow: An idealized modeling study with a straight jet. *Quart. J. Roy. Meteor. Soc.,* **134,** 69–91.

Saha, S., and Coauthors, 2010: The NCEP Climate Forecast System Reanalysis. *Bull. Amer. Meteor. Soc.,* **91,** 1015–1057.

Schumacher, R. S., and R. H. Johnson, 2005: Organization and environmental properties of extreme-rain-producing mesoscale convective systems. *Mon. Wea. Rev.,* **133,** 961–976.

——, and C. A. Davis, 2010: Ensemble-based forecast uncertainty analysis of diverse heavy rainfall events. *Wea. Forecasting,* **25,** 1103–1122.

——, and T. J. Galarneau Jr., 2012: Moisture transport into midlatitudes ahead of recurving tropical cyclones and its relevance in two predecessor rain events. *Mon. Wea. Rev.,* **140,** 1810–1827.

——, ——, and L. F. Bosart, 2011: Distant effects of a recurving tropical cyclone on rainfall in a midlatitude convective system: A high-impact predecessor rain event. *Mon. Wea. Rev.,* **139,** 650–667.

Sinclair, M. R., 2002: Extratropical transition of southwest Pacific tropical cyclones. Part I: Climatology and mean structure changes. *Mon. Wea. Rev.,* **130,** 590–609.

Srock, A. F., and L. F. Bosart, 2009: Heavy precipitation associated with southern Appalachian cold-air damming and Carolina coastal frontogenesis in advance of weak landfalling Tropical Storm Marco (1990). *Mon. Wea. Rev.,* **137,** 2448–2470.

Trier, S. B., and D. B. Parsons, 1993: Evolution of environmental conditions preceding the development of a nocturnal mesoscale convective complex. *Mon. Wea. Rev.,* **121,** 1078–1098.

Wang, Y., Y. Wang, and H. Fudeyasu, 2009: The role of Typhoon Songda (2004) in producing distantly located heavy rainfall in Japan. *Mon. Wea. Rev.,* **137,** 3699–3716.

Wilks, D. S., 2006: *Statistical Methods in the Atmospheric Sciences*. 2nd ed. Academic Press, 627 pp.